Axon morphogenesis and maintenance require an evolutionary conserved safeguard function of Wnk kinases antagonizing Sarm and Axed

Azadeh Izadifar, Julien Courchet, Daniel Virga, Tine Verreet, Stevie Hamilton, Derya Ayaz, Anke Misbaer, Sofie Vandenbogaerde, Laloe Monteiro, Milan Petrovic, et al.

Version of Record: https://www.sciencedirect.com/science/article/pii/S0896627321005055
Manuscript_a8b8348bd8375da415d7189eb4550d3c

Axon morphogenesis and maintenance require an evolutionary conserved safeguard function of Wnk kinases antagonizing Sarm and Axed

Azadeh Izadifar[1,2,3*], Julien Courchet[4,5* #], Daniel M. Virga[5], Tine Verreet[2,3], Stevie Hamilton[5], Derya Ayaz[2,3], Anke Misbaer[2,3], Sofie Vandenbogaerde[2,3], Laloe Monteiro[4], Milan Petrovic[2,3], Sonja Sachse[2,3], Bing Yan[2,3], Maria-Luise Erfurth[2,3], Dan Dascenco[2,3], Yoshiaki Kise[7], Jiekun Yan[2,3], Gabriela Edwards-Faret[1,2,3], Tommy Lewis[5,8], Franck Polleux[5,6,#] and Dietmar Schmucker[1,2,3,#,&]

* Equal contribution

Co-corresponding authors

& Lead Contact

[1] Life and Medical Sciences Institute (LIMES), Bonn, Germany

[2] VIB Center for Brain & Disease Research, Leuven, Belgium

[3] KU Leuven, Department of Neurosciences, Leuven, Belgium

[4] Univ Lyon, Université Claude Bernard Lyon 1, CNRS UMR-5310, INSERM U-1217, Institut NeuroMyoGène, F-69622, Villeurbanne, France

[5] Department of Neuroscience, Mortimer B. Zuckerman Mind Brain Behavior Institute, Columbia University, New York, NY- USA

[6] Kavli Institute for Brain Science, Columbia University, New York, NY -USA

[7] University of Tokyo, Japan

[8] Aging & Metabolism Program, Oklahoma Medical Research Foundation, Oklahoma City, OK-USA

Address correspondence to:
dslab@uni-bonn.de
fp2304@columbia.edu
julien.courchet@univ-lyon1.fr

SUMMARY

The molecular and cellular mechanisms underlying complex axon morphogenesis are still poorly understood. We report a novel, evolutionary conserved function for the *Drosophila* Wnk kinase (dWnk) and its mammalian orthologs, WNK1 and 2, in axon branching. We uncover that dWnk, together with the neuroprotective factor Nmnat, antagonizes the axon destabilizing factors D-Sarm and Axundead (Axed) during axon branch growth, revealing a developmental function for these proteins. Overexpression of D-Sarm or Axed result in axon branching defects, which can be blocked by overexpression of dWnk or Nmnat. Surprisingly, Wnk kinases are also required for axon maintenance of adult *Drosophila* and mouse cortical pyramidal neurons. Requirement of Wnk for axon maintenance is independent of its developmental function. Inactivation of dWnk or mouse Wnk1/2 in mature neurons, leads to axon degeneration in the adult brain. Therefore, Wnk kinases are novel signaling components that provide a safeguard function in both developing and adult axons.

INTRODUCTION

A hallmark in the generation of neuronal cell type diversity is the acquisition of diverse morphologies, which requires the formation of axonal and dendritic compartments ranging from simple to highly complex depending on the degree of neurite branching. Specifying the degree and pattern of neurite branching is crucial in brain development as it directly impacts the total number and spatial distribution of synaptic contacts of each circuit element (Courchet et al. 2013; Iascone et al. 2020; Chia et al. 2014; Urwyler et al. 2019). However, the identity of the molecular effectors determining how diverse, cell-type specific, patterns of axon arborization are established and how they are stabilized as well as maintained throughout the life of an organism remains a major challenge (Südhof 2017).

We performed a reverse genetic screen to identify novel regulators of axon branching by utilizing an experimental system in *Drosophila* that combines efficient single neuron labeling and simultaneous knockdown of candidate genes (Urwyler et al. 2019). Clear orthologues of selective candidates were then further examined in vertebrates. Using this approach, we found that loss of the *Drosophila* dWnk kinase specifically disrupts axon growth and branch patterning of mechanosensory neurons. Surprisingly, unlike other essential regulators of axon branching (Sudarsanam et al. 2020; He et al. 2014; Dascenco et al. 2015; Lewis,

Courchet, and Polleux 2013), we discovered that dWnk is also continuously required in mature neurons for axon maintenance. Moreover, comparative studies in mouse cortical pyramidal neurons (PNs) provide strong evidence that both of these functions of Wnk kinases are conserved and required in PNs, i.e. long-range projecting mammalian neurons of the central nervous system (CNS).

Wnk kinases are present in most multicellular organisms including plants and some unicellular organisms but not in yeast (Hoorn et al. 2011; McCormick and Ellison 2011). Mammals have four Wnk kinases (WNK1-4) and *Drosophila* one (dWnk). The WNK ("With No K(Lysine)") kinases are catalytically active but are referred to as 'atypical kinases' because a catalytically important lysine residue is swapped from subdomain II to subdomain I (Xu et al. 2000; Veríssimo and Jordan 2001). WNK proteins are involved in a broad spectrum of diseases (e.g. hypertension, sensory and autonomic neuropathy, osteoporosis and many different cancers (McCormick and Ellison 2011; Alessi et al. 2014; Siew and O'Shaughnessy 2013; Sato and Shibuya 2018).

The majority of studies on human WNK kinases have been conducted in the context of blood pressure regulation, due to the identification of mutations in human patients with hereditary hypertension (Familial Hyperkalemia and Hypertension (FHHt) or Gordon's Syndrome) (Wilson et al. 2001). For this reason, a major focus in dissecting WNK function has been on studying renal regulation of ion transport (Alessi et al. 2014; Yang et al. 2003; Pela 2012; Vidal-Petiot et al. 2013; Jun et al. 2009; Costa et al. 2015). However, regulation of ion homeostasis is only one of multiple functions of WNK kinases (Siew and O'Shaughnessy 2013; Gallolu Kankanamalage, Karra, and Cobb 2018) and they are broadly expressed, including in the developing as well as mature brain. In rare cases WNK function has been linked to a severe form of peripheral sensory neuropathy (HSNA2) (Lafreniere et al. 2004; Rivière et al. 2004; Roddier et al. 2005; Coen et al. 2006), however their developmental, cellular and molecular mechanisms are poorly understood in neurons. The fact, however, that most identified mutations cluster in a neuron-specific alternatively spliced exon (HSN2) of human Wnk1, supports the notion that Wnk1 kinase plays an important role in sensory neurons (Shekarabi et al. 2008; Yuan et al. 2017; Rahmani et al. 2018)

In the process of studying the role of dWnk kinase in fly sensory neurons, we identified novel interactors of Wnk kinases. Specifically, we found that nicotinamide mononucleotide adenylyltransferase (Nmnat), Sarm and Axundead (Axed) are molecular interactors of dWnk. While Nmnat is required for axon maintenance, Sarm and Axed are primarily studied for their roles as effectors in active axon degeneration (e.g. in Wallerian Degeneration) in response to axon injury (Coleman and Freeman 2010; Gilley and Coleman 2010; Neukomm et al. 2017; Osterloh et al. 2012). We provide evidence that dWnk and Nmnat have synergistic functions in axon growth and branching but are also required in post-developmental

processes to continuously support axon maintenance. The function of dWnk is evolutionarily conserved, as their mouse orthologues WNK1 and WNK2 are both required in cortical pyramidal neurons (PNs) during axon morphogenesis as well as maintenance. Genetic epistasis analysis demonstrates that both dWnk and Nmnat functions during axon development and axon maintenance are mediated by antagonizing the axon destruction function of Sarm and Axed. Depletion of axon protective factors (e.g. dWnk/WNK1/2, Nmnat) during development leads to axon branching defects, whereas their depletion in mature neurons eliminates their safeguard function and initiates spontaneous axon degeneration in the absence of axon injury.

RESULTS

Wnk is required for axonal branch patterning in fly mechanosensory neurons

To identify signaling factors regulating axon branching during central nervous system (CNS) development, we focused on the central projections of *Drosophila* mechanosensory neurons that innervate sensory bristles of the adult fly thorax (**Fig. 1A-B**). Mechanosensory neurons from the central domain of the thorax all extend axonal projections to the ventral nerve cord (VNC) where they establish a cell type-specific and stereotyped axonal branching pattern (Chen et al. 2006). Single cell labeling using either lipophilic dye fills (Chen et al. 2006) or genetic mosaic labeling (He et al. 2014; Urwyler et al. 2015) allows the visualization of the precise axonal branching pattern within the VNC (**Fig. 1B,D**).

In a reverse genetic screen, we examined the potential role of the majority of *Drosophila* kinases as well as phosphatases (Dascenco et al. 2015) and found that RNAi-mediated knockdown of *Drosophila* Wnk kinase (dWnk) leads to a rather unique phenotype characterized by strong impairment of axonal branching of many mechanosensory axon projections (**Fig. 1B-C**). Specifically, knockdown of dWnk in posterior scutellar (pSC) mechanosensory neurons strongly impaired axon collateral formation and patterning within the *Drosophila* CNS (**Fig. 1D-F**). In mutant axons, extensions of collaterals along the long posterior and contralateral projections were almost absent. Instead, a plexus of unpatterned and seemingly randomly projecting short axon branches were formed (**Fig. 1E-F)**.

We next examined two dWnk loss of function (LOF) alleles (Wnk^{G1286} and Wnk^{F1183}) using mosaic analysis with a repressible cell marker (MARCM). These LOF alleles harbor EMS-induced point mutations resulting in strong (Wnk^{G1286}) or complete (Wnk^{F1183}) LOF (**Fig. S1**) and have previously been characterized (Berger et al. 2008). Anti-Wnk antibodies show that dWnk is broadly expressed throughout the nervous system (**Fig. S1D-F** and **Fig. S2A-D**) and absent in homozygous Wnk^{F1183} animals (**Fig. S1B-G**). Immunostaining reveals that

endogenous dWnk protein localize to the cytoplasm and also throughout axonal processes including growth cones (**Fig. S2E-H**). Single cell labeling in both homozygous mutant pSc neurons (**Fig. 1G-H**) revealed qualitatively similar axon branching defects as found by RNAi-mediated knock-down of dWnk (**Fig. 1E-F**). These defects were substantially rescued cell-autonomously by overexpression of *dWnk* cDNA in mechanosensory neurons (**Fig. 1I**). Moreover, an analogous analysis of a functionally similar yet different mechanosensory neuron, the posterior dorsocentral neuron (pDc), (**Fig. 1A**) revealed similar defects of axon branching as found in pSc neurons (**Fig. 1J-M**). Moreover, analysis of other neurons types using knock-down or LOF alleles revealed a strong requirement of dWnk in olfactory sensory neurons with defects in axon growth, branching and targeting (**Fig. S3A-F**). In addition to these requirements in sensory neurons, dWnk is also required in interneurons of the visual system (DCN) (**Fig. S3G-H**). Analysis of DCN neurons suggests the possibility that dWnk is primarily important for axon branch extension within the target area but not in growth or branching of the dendritic compartment. Analysis of MARCM clones of DCN neurons in adult flies (**Fig. S3I-J)** as well as clones of dorsal arborization neurons (ddaE-class I sensory neurons) in larvae did not reveal any defects in dendrite patterning of these neurons (**Fig. S3K-L**). Taken together this suggests a cell-autonomous requirement of *Drosophila Wnk* in multiple sensory and interneuron types and that this function is specific to axon morphogenesis.

Loss of dWnk in mechanosensory neurons leads to early onset axon degeneration in adult flies

The phenotypic effects on axon branching characterizing dWnk RNAi knock-down or MARCM clones for strong loss of function alleles were similar (**Fig. 1C, E-H** and **K-M**). However, we noted that many samples of flies with Wnk^{G1286} or Wnk^{F1183} mutant mechanosensory neurons and in particular samples older than 2 days (post-eclosion) had no axonal projections within the VNC target area (**Fig. 2**).

We, therefore, determined quantitatively the number of samples where mutant axons had reached the VNC in adult flies at different time points post-eclosion (**Fig. 2D-H**). Within the first 24 hours (<Day 1) after eclosion, ~40% of Wnk^{F1183} and ~80% of Wnk^{G1286} mutant neurons still had central axonal projections in the VNC. In all samples where an axon was present in the VNC target area, we observed strong axon branching defects similar to the RNAi knock-down samples (**Fig. 2D-F**). In older adult flies, however, no axon or only traces of remaining axon branches were detectable in Wnk^{F1183} mutant neurons and very few in Wnk^{G1286} mutant neurons (**Fig. 2G-H**) suggesting a progressive loss of axons over time.

In contrast, either at Day1 or in older flies, we never observed a loss of axons in the VNC of flies expressing a single-copy of UAS-dWnk RNAi (dWnk $RNAi^{1X}$), despite strong and highly

penetrant axon branching defects (**Fig. 1E;** left panel of **Fig. 2H**). Therefore, we examined whether enhancing the RNAi-mediated knock-down of dWnk would initiate degeneration. Indeed, using two copies of UAS-dWnk RNAi (dWnk RNAi^{2X}) did lead to a 50% reduction of distal axons in the respective samples compared to controls or single-copy UAS-dWnk RNAi (**Fig. 2H**). These results suggest a dose-dependence of dWnk expression for proper axon maintenance in mechanosensory neurons. However, the axon branching defects displayed little phenotypic variability since they were observed in all RNAi or LOF alleles examined (see above; **Fig. 1** and left panel of **Fig. 2H**). In contrast, the degeneration following the loss of dWnk function, showed significant allelic differences, appeared to be progressive, and only in mutants carrying the strongest loss of dWnk allele, all axons had degenerated in three days or older flies (**Fig. 2H**).

To better characterize the progressive nature of the axon degeneration phenotype due to dWnk LOF, we took advantage of the fact that we could visualize and identify the proximal part of the main axon (unbranched axon) close to the cell body (**Fig. 2A** and **C**) through the thin cuticle of the thorax by using single neuron GFP-expression and antibody-based detection of microtubule organization (using anti-22C10 antibody against Futsch, a microtubule-associated protein in *Drosophila* neurons) (**Fig. 2C**). We examined wild type and dWnk mutant neurons (dendrite, soma, and axon) in the scutellar part of adult flies (**Fig. 2I-N**).

We detected a near continuous labeling of the axon and microtubule cytoskeleton using membrane-tethered CD8-GFP and anti-22C10 antibody staining in wild type control samples (**Fig. 2I** and **M**). In contrast, dWnk mutant neurons showed moderate signs of axonal degeneration already in one day old flies (**Fig. 2J**). In particular, in mutant neurons with strong dWnk LOF, the severity of axonal defects correlated with the age of the flies (**Fig. 2L** and **N**). In 3 days old mutant neurons, we often detected only segments of the most proximal axon, while membrane blebbing and loss of cytoskeletal integrity was prominent (**Fig. 2N**). These results provide evidence that loss of dWnk in mechanosensory neurons triggers progressive and spontaneous axon degeneration.

It seems plausible that the distal axon branching defects within the VNC lead directly to axon degeneration, possibly as a consequence of losing target-derived trophic support once these mechanosensory axons reached the CNS.

Nevertheless, to test more directly an adult-specific requirement for axon maintenance, we induced RNAi-dependent knockdown of dWnk following the completion of axon branching at the end of pupal stages (**Fig. S4A-B**). We used temperature shifts to control the timing of RNAi expression such that dWnk expression is either absent during larval and early pupal stages which reproduced the axon branching followed by axon degeneration as shown above (**Fig. S4B-E**) or present during the developmental phase of axon growth and

branching but absent starting at late pupal and adult stages (**Fig. S4B-C, F-G**). Indeed, the latter manipulation i.e. a late knock-down of dWnk did not disrupt the axon branch patterning at early stages (**Fig. S4B-C** and **F**) but clearly triggered axon degeneration of adult mechanosensory neurons 3-5 days after hatching (**Fig. S4G**). This temporal dissection of dWnk knockdown supports the model of a requirement of adult expression of dWnk for axon maintenance, independent of its role in axon development.

In summary, dWnk mutant mechanosensory axons can grow from the periphery to the VNC but require dWnk function during axonal branch growth and patterning of its arborization in the VNC target area.

Loss of dWnk impairs axonal branch extension/stabilization during early developmental stages

In order to better characterize the role of dWnk during axon morphogenesis we analyzed axon growth at multiple time points (2-hour time windows) during pupal development (**Fig. 3A**). In wild type animals, axon extension into the VNC is completed before 30hrs of pupal development. At this time point, unpatterned axon sprouting is initiated. Subsequent branch extensions, consolidation, and selective primary collateral formation proceed within the next 10 hours (**Fig. 3A-G**). In contrast, Wnk knock down (Wnk RNAi^{2X}) (**Fig. 3H-M)** or Wnk mutants axons (Wnk LOF) (**Fig. 3N-S**) show an abnormal axon morphogenesis starting at the early sprouting stage, where a strong reduction in filopodial extensions is already visible at 30 hrs of pupal development. Throughout the entire axon branching period, we detected a reduction of the overall number of filopodia (**Fig. 3T**). At subsequent stages, axon branches grow and continue to extend but follow erroneous paths and with strong deficits in spatial patterning of axon collaterals (**Fig. 3 J-M; P-S**). We observed these mutant phenotypes with abnormal axon growth and branch patterning using knock-down or MARCM analysis of null mutant neurons. These results exclude the possibility that mechanosensory axons might first develop normally but then regress by limited degeneration of terminal axon branches. In contrast, they support a requirement of dWnk in filopodial and axon branch extension/stabilization as well as axon branch guidance.

Wnk function in axonal morphogenesis is conserved in mouse cortical pyramidal neurons

dWnk has four related orthologs in mammals named WNK1-4 and several studies have shown that in particular WNK1 and WNK4 have prominent roles in the regulation of ion homeostasis in mammalian kidneys (Richardson et al. 2008; Shekarabi et al. 2008; Shekarabi et al. 2017). Given the striking neurodevelopmental defects due to loss of dWnk in mutant *Drosophila* neurons, we investigated if mammalian WNK kinases play evolutionary

conserved roles in axon branching and axon maintenance using mouse cortical pyramidal neurons (PNs), which are long-range projecting principal glutamatergic neurons in the mammalian cortex.

Using a public database (Genepaint) for mRNA expression by *in situ* hybridization (ISH) in mouse embryo at embryonic day (E)14.5, *Wnk1* mRNA displays a ubiquitous expression and is expressed strongly in the periventricular region of the developing brain including the cortex (arrow in **Fig. S5A**). *Wnk2* mRNA expression is largely restricted to the CNS with high expression in the developing cortex (arrow in **Fig. S5B**). *Wnk3* and *Wnk4* were not detected by ISH in the developing CNS at E14.5 (**Fig. S5C-D**). Interestingly, the same general trend was found in adult mouse brain using a different database (Allen Brain Institute), where ISH revealed that *Wnk1* and *Wnk2* are expressed broadly in all regions of the central nervous system (CNS) but *Wnk3-4* mRNA are not detectable (**Fig. S5E-H**). Finally, to determine if the same trend of adult expression found in mouse brain applied to various cell types in the adult human cortex, we used a publicly available single cell RNA sequencing (scRNAseq) database (UCSC Cell Browser). This revealed the same trend as in adult mouse brain showing that in the human cortex, *WNK1* and *WNK2* share a highly similar cell type expression pattern being most abundant in principal pyramidal neurons from layer 2/3, 4 and 5/6 as well as in cortical interneuron sub-populations and some non-neuronal cell types (**Fig. S6A-B**), whereas *WNK3* and *WNK4* are almost completely absent from any adult human cortical cell types (**Fig. S6C-D**).

To investigate whether the mouse *Wnk1* and/or *Wnk2* are required for axon growth and branching of cortical pyramidal neurons (PNs), we performed *in utero* cortical electroporation (IUCE) of shRNA encoding plasmids targeting *Wnk1* or *Wnk2* (**Fig. S7**) at embryonic days E15.5, in order to target cortico-cortical projecting layer 2/3 PNs in the primary somatosensory cortex. Brains of electroporated mice were harvested at various postnatal stages: (1) at postnatal day (P)10, an immature stage when axons have reached the contralateral hemisphere but just started to defasciculate and invade the cortex where they are still undergoing terminal branching (**Fig. 4A**), (2) at P15, an intermediate stage where axons are progressively increasing their branching in their target layers 2/3 and 5 (**Fig. 4B**), P21, a juvenile stage with adult-like terminal branching of callosal axons (**Fig. 4C**) and at P35, an adult stage. In layer 2/3 PNs expressing either *Wnk1* shRNA (**Fig. 4E-H**) or *Wnk2* shRNA (**Fig. 4I-L**), a population of axons reach the contralateral hemisphere at P10 (**Fig. 4E and I**) but terminal axon branching is severely affected through the intermediate stages (**Fig. 4F-G and J-K**), never reaching wild-type control levels even at adult stages with only a few axons left at P35 (**Fig. 4H** and **L**). Quantification of the optical density from tdTomato+ axons throughout all cortical layers normalized by the total number of electroporated cell body of layer 2/3 PNs on the ipsilateral side demonstrates that *Wnk1* or *Wnk2* shRNA expressing

axons are severely reduced on the contralateral side compared to control shRNA expressing axons at all stages examined (**Fig. 4M-P**).

Analysis of axon density at the midline (corpus callosum) in *Wnk1* or *Wnk2* shRNA expressing neurons confirm that axons successfully cross the midline and are present from P10 to P21 but show significant reduction in number by P35 compared to control (**Fig. S8A-L**).

To quantify axon growth and branching at single cell resolution, we turned to *ex utero* cortical electroporation (EUCE) followed by dissociated culture *in vitro* as previously described (Courchet et al. 2013). We compared axon morphology in control, WNK1 overexpression (WNK1-OE) as well as *Wnk1* or *Wnk2* shRNA-mediated knockdown conditions. Compared to control neurons, overexpression of WNK1 led to longer axons, with more collateral branches (**Fig. S9A-B**). Conversely, shRNA-mediated knockdown of either *Wnk1* or *Wnk2* resulted in cortical PNs with shorter and less branched axons (**Fig. S9C-D**). Quantifications confirmed a dose-dependent effect of WNK1 on axon length and collateral branching (**Fig. S9E-G**). *Wnk1* or *Wnk2* knockdown led to a similar reduction of axon length and collateral branching without any additive effect of the double knockdown of *Wnk1* and *Wnk2* (**Fig. S9H-J**), suggesting they belong to the same pathway. Interestingly effect of *Wnk1* knockdown or over-expression are restricted to axon morphogenesis since we did not observe any consequence of *Wnk1* modulation (WNK1 overexpression or *Wnk1* knockdown) on dendritic morphology at 21DIV (**Fig. S9-K-M**). This is consistent with results presented above (**Fig. S3I-L**) showing that loss of dWnk in *Drosophila* DCN and sensory ddaE-Class I neurons lead to strong axonal but no dendritic morphogenesis defects within the same neurons.

To further confirm that WNK1 and WNK2 affect axon growth and branching, we performed time-lapse imaging of axonal development over 16 hours (10 minutes imaging interval) and quantified axon elongation and branch formation (**Fig. S10A-B**). Axon elongation was disrupted by a failure to consolidate growth at the tip of the axon. Indeed, short periods of growth cone progression (**Fig. S10C**, green arrowhead) alternated with growth cone retraction (purple arrowhead) and initiation of an alternative growth cone from an above position on the axon shaft. Although the growth cone speed during the periods of growth was identical in control and knockdown condition, we measured a reduced time spent growing and increased pause duration in *Wnk1* and *Wnk2* knockdown neurons, resulting in a net decrease of axon elongation (**Fig. S10D-G**). Finally, we measured that branch dynamics were altered with a decrease of the fraction of new, stable branches created, and an increase in transient (<2hours) branches (**Fig. S10H**). Altogether these results demonstrate that mouse WNK1 and WNK2 are directly involved in axon development similarly to their *Drosophila* counterpart.

Wnk1/2 are required in axon maintenance in developing neurons

Following expression of Wnk1 or Wnk2 shRNA, we observed a gradual, significant reduction in mVenus+ axonal labeling in the corpus callosum at the midline compared to control shRNA (**Fig. S8A-L**) and a marked loss of axon branching both *in vivo* (**Fig. 4**) and *in vitro* at least at early stages of neuronal differentiation (**Fig. S9**). These data suggest that *Wnk1* or *Wnk2* are not only required for axon branching but might also be required for axon maintenance.

We used very sparse EUCE in order to obtain individual cortical PNs that can be optically-isolated and performed time-lapse analysis by repetitively imaging individual neurons once every 24hr from 5 to 10DIV (**Fig. 5A**). In cortical PNs expressing control shRNA, we observed progressive but extensive axon growth and branching (**Fig. 5A** and **F-G;** see **Movies S1-S2**) but never spontaneous axon fragmentation and degeneration in these culture conditions.

Cortical PNs expressing *Wnk1* or *Wnk2* shRNA, display two classes of phenotypes: in ~55% cortical PNs expressing *Wnk1* shRNA (**Fig. 5B**) and ~65% of cortical PNs expressing *Wnk2* shRNA (**Fig. 5C**), we observed reduced axon growth and branching but no sign of axon fragmentation or degeneration at least by 10 DIV (**Fig. 5F**; see also **Movies S3 and S5**). Furthermore, in the remaining ~45% of cortical PNs expressing *Wnk1* shRNA and ~35% of cortical PNs expressing *Wnk2* shRNA, we observed initially reduced axon growth and branching followed by striking patterns of rapid axon fragmentation/degeneration occurring between 7-8 DIV (**Fig. 5D-F; Movies S4** and **S6**). Quantification of the dynamics of axon growth and branching (cumulative axon length/area **Fig. 5G** and **I**) or normalized growth rate (increase in total axonal length per day; (**Fig. 5H** and **J**)) demonstrated that axon growth and branching is significantly reduced in axons expressing *Wnk1* or *Wnk2* shRNA in both classes of axons.

Our *ex utero* electroporation protocol is performed in both cases at E15 targeting the progenitors lining the ventricular zone at that time which generate exclusively layer 2/3 pyramidal neurons in the dorsal telencephalon. However, the limitation of this approach is that, upon electroporation, the neural progenitors pick up various amount of the plasmid and subsequently can divide several times to generate layer 2/3 PNs thereby creating a 'mosaic' expression of cDNA or shRNA encoding plasmids. We favor this explanation to describe the range of phenotypes obtained leading to two extreme phenotypes upon Wnk1 or Wnk2 shRNA mediated knockdown: (1) one class of neurons where axon branching/growth is affected but not axon maintenance (presumably the neurons where knock down of Wnk1 or 2 is suboptimal) and (2) a second class of neurons where axon branching and maintenance is affected (presumably the neurons where knock down of Wnk1 or 2 is above a certain

threshold). This interpretation is reinforced by the analysis performed in *Drosophila* where neurons expressing 1x RNAi (expressed genomically here) show severe axon branching defect but not axon degeneration and neurons expressing 2x RNAi show initially axon branching defects but ultimately axon degeneration (**Fig. 2**).

Wnk1/2 are required for axon maintenance in adult neurons

In order to directly test if Wnk1 and Wnk2 are required for axon maintenance in adult mouse cortical pyramidal neurons, we developed a new experimental approach that enables inducible expression of shRNA *in vivo*. Our strategy revolves around two parts (**Fig. 6A-B**): (1) we used IUCE (E15) to co-express a plasmid expressing a tamoxifen inducible form of Cre (ERT2-Cre-ERT2) and a novel plasmid expressing the red fluorophore mStrawberry in the absence of tamoxifen but upon tamoxifen-dependent Cre activation, the CAG promoter/enhancer cassette orientation is flipped leading to expression of a bi-cistronic mRNA encoding EGFP and a Wnk1 or Wnk2 shRNA upon mRNA processing (**Fig. 6A**). We performed tamoxifen induction of Cre-mediated recombination (and induced shRNA expression) using four daily tamoxifen intraperitoneal (IP) injections at P30-33. This approach is robust because in the absence of tamoxifen, we observed many mStrawberry expressing layer 2/3 PNs (**Fig. 6C**) but we never EGFP co-expressing neurons (**Fig. 6D**; see also **Fig. 6G** and **P**). However, in mice injected with Tamoxifen, we observed a large fraction of layer 2/3 PNs co-expressing EGFP at various levels (~30-50% co-expression) (**Fig. 6E-F)**. This approach therefore allowed us to test if inducible shRNA knockdown of Wnk1 or Wnk2 in adult layer 2/3 PNs is required for axon maintenance. Seven days following the first tamoxifen injection (i.e. at P37) or injection of vehicle (corn oil) for the control group, we imaged axons of layer 2/3 PNs at the midline (corpus callosum) or on the contralateral side where they undergo terminal axon branching. Both Wnk1 and Wnk2 shRNA expression leads to significant reduction of the fraction of axons relative to the number of electroporated neurons at the corpus callosum (**Fig. 6K** and **T**) and on the contralateral side (**Fig. 6L** and **U**) compared to control (**Fig. 6H-I** and **6Q-R**). Quantification of optical density of mStrawberry+ axons on the contralateral side (normalized to number of electroporated neurons) demonstrate a significant reduction in axon density in Wnk1 shRNA expressing neurons (**Fig. 6M**) or Wnk2 shRNA expressing neurons (**Fig. 6V**) compared to control. The same significant reduction in optical density of mStrawberry+ axons at the midline is observed in Wnk1 or Wnk2 shRNA expressing axons compared to control (**Fig. 6N** and **W**). These results demonstrate that Wnk1 and Wnk2 are required for axon maintenance in adult mouse pyramidal neurons.

Loss of Nmnat and gain of dSarm or Axed disrupt axon branching during development

Mammalian WNK1 and WNK4 are known to regulate the downstream kinase OSR1/SPAK and target the sodium/potassium transporters NCC/KCC in kidney cells (Vitari et al. 2005; Moriguchi et al. 2005; Anselmo et al. 2006; Gagnon, England, and Delpire 2006). This regulation is essential for blood pressure regulation (Richardson and Alessi 2008; Wu, Wolley, and Stowasser 2019; Hadchouel, Ellison, and Gamba 2016). Disruption of these WNK-dependent functions constitutes the basis of hypertension in several hereditary human diseases (Rafiqi et al. 2010). In order to explore the molecular mechanisms underlying WNK function in axon branching and degeneration, we initially tested if downregulation of Frayed, the *Drosophila* ortholog of OSR/SPAK kinases, or NCC/KCC phenocopied dWnk LOF axon branching defects. However, we could not detect dWnk-like axonal branching defects upon RNAi knock-down of Frayed or KCC (**Fig. S11**).

In our efforts to identify other potential factors mediating the function of dWnk, we tested previously identified effectors of axon maintenance (Gilley and Coleman 2010; Neukomm et al. 2017; Babetto et al. 2013; Conforti, Gilley, and Coleman 2014; Essuman et al. 2017). In a candidate screen, we discovered that loss of function and RNAi knockdown of Nmnat in mechanosensory neurons leads to axon branching defects remarkably similar to dWnk loss of function defects (**Fig. 7A and C-E**). A previous study provided evidence that reduction of Nmnat in *Drosophila* sensory neurons leads to activation of dSarm as well as a newly identified protein Axundead (Axed) to execute axon degeneration (Neukomm et al. 2017). Consistent with these findings, we found that overexpression of Axed or dSarm caused axon branching defects similar to loss of dWnk or loss of Nmnat (**Fig. 7F-G**). These results provide evidence that Nmnat is required developmentally for axon branching of mechanosensory neurons. Moreover, overexpression of Axed or dSarm during axon development resulted in axon branching defects remarkably similar to loss of dWnk or Nmnat.

dWnk regulates axon branching and maintenance by regulating Nmnat, dSarm, and Axed

In order to address the functional relationship of dWnk and these components we used genetic epistasis analysis (**Fig. 7; Fig. S12**). We found that both loss of Axed and dSarm can suppress the axon branching defects in dWnk mutant neurons (**Fig. 7 C, I, J** and **O; Fig. S12 A-E** and **Q**) and prevents loss of axons (**Fig. 7S-T, W** and **X; Fig. S12 K-M** and **R**). Conversely, the gain of function branching defects and loss of axons upon Axed and dSarm overexpression can be suppressed by co-overexpression of dWnk (**Fig. 7F-G, M-N** and **O; Fig. S12F-J, N-P and R**). This argues for an antagonistic functional relation between dWnk

and the axon destruction factors Axed and dSarm during axon branching as well as maintenance.

Overexpression of dWnk or Nmnat alone did not result in any dominant phenotypic defects (**Fig. 7B** and **H**). However, we found that the axon branching defects characteristic for dWnk mutant neurons can be suppressed by Nmnat overexpression (**Fig. 7C, H, K** and **O**). Conversely, axon branching defects characterizing Nmnat RNAi knock-down neurons can be rescued by overexpression of dWnk (**Fig. 7E, L** and **O**). We further observed that overexpression of Nmnat in pSc neurons can also suppress or slow down the degeneration of axons in dWnk mutant neurons (**Fig. 7P-R, U-V** and **X**). In summary, the genetic analysis of fly mechanosensory neurons suggest that dWnk functions synergistically with Nmnat in order to prevent gain of activity of dSarm and Axed, which can disrupt both: (i) axon branching during development and (ii) axon maintenance in mature neurons.

Wnk and Nmnat proteins can form complexes and are depleted by Sarm1 activity

We conducted a series of biochemical immunoprecipitations to test potential protein interactions of dWnk as well as mammalian WNK1/2 with the axon maintenance/destruction factors examined in the genetic analysis. (**Fig. 8**). We found that immunoprecipitation of endogenous dWnk from S2 cell extracts can pull down tagged-dNmnat (**Fig. 8A**). This is consistent with published findings, where dWnk was identified by mass spectrometry from a complex co-purified with Nmnat overexpressed in fly brains (Ali et al. 2016). For the mammalian homologs Wnk1/2 we found that Nmnat2 can be co-immunoprecipitated with Wnk1, suggesting conserved Wnk-Nmnat interactions. We found that these interactions are likely occurring via the N-terminal part of Wnk1 and to a lesser degree with the kinase domain of Wnk1 itself (**Fig. 8B**). We further found that Wnk1 can be immunoprecipitated with Wnk2 and vice versa (**Fig. 8C**) consistent with the finding that both kinases are functionally required in mouse PNs.

We further tested potential dWnk interactions with the axon destructive factors Axed and dSarm. We found that co-expressed Axed (V5-tagged) and dWnk could form complexes in *Drosophila* S2 cells (**Fig. S13A**). *Drosophila* Axed is a member of the large BTB-domain containing family of proteins. While currently no functional mammalian orthologue is known, we found that mammalian Wnk2 has the potential to interact with *Drosophila* Axed and a subset of related BTB-domain containing proteins (**Fig. S13B-F**). In contrast, the functional conservation of *Drosophila* dSarm and mammalian Sarm1 is well documented by molecular and genetic studies. We, therefore, tested the potential molecular interactions of the axon-protective WNK1/2 kinases and degeneration effector SARM1. Surprisingly however, co-overexpression of SARM1 with either WNK1 or WNK2 caused a strong decrease in both WNK1 or WNK2 protein abundance (**Fig. 8 D** and **G**). Yet by testing different expression

levels of SARM1 and WNK1 or WNK2, we nevertheless, were able to co-immunoprecipitate SARM1 and WNK1 or WNK2 (**Fig. S14A-B**). Importantly, the co-expression experiments revealed not only that SARM1 protein over-expression either directly or indirectly triggers rapid depletion of WNK1 and WNK2 in HEK293T (**Fig. 8D**), (Quantification in **Fig. 8G**), or SH-SY5Y cells (**Fig. S14B**), but also that NMNAT1 as well as NMNAT2 levels were nearly completely depleted when co-expressed with SARM1 (**Fig. 8E-F**), (Quantification in **Fig. 8G**). Application of commonly used inhibitors of proteasomal degradation to cells co-expressing Sarm1 and Wnk2 or Nmnat2 did not block this depletion of Wnk2 and Nmnat2 protein (**Fig. S14B**). We further detected no decrease in mRNA expression of Wnk1/2 or Nmnat1/2 upon overexpression of Sarm1 (**Fig.S14C**). It has been reported that Nmnat2 protein is labile and has a rapid turnover time whereas the mutant (and axon-protective) Nmnat-fusion protein Wallerian degeneration slow (WldS), is significantly more stable (Coleman and Freeman 2010). Consistent with previous reports and this hypothesis we found that blocking *de novo* protein synthesis in cells expressing Nmnat2 by addition of cycloheximide, Nmnat2 protein but not WldS is rapidly lost (**Fig. S14E**). Importantly, Nmnat2 depletion is also more sensitive to Sarm1 overexpression than WldS. We, therefore, hypothesize that one potential mechanism by which Sarm1 could trigger depletion of Wnk or Nmnat proteins is through inhibition of *de novo* protein synthesis. The direct target of Sarm1 underlying this translational control is currently not known. However, testing different mutant forms of Sarm1 provided evidence that this potential translational control function of Sarm1 requires it catalytic NAD+ consuming function (**Fig. 8H-I**). Specifically, we co-expressed Wnk1 (**Fig. 8H**) and Wnk2 (**Fig. 8I**) with Sarm1 protein forms that enhance or lack catalytic activity. We found that dominant active Sarm1 mutants are even more potent than wild type Sarm1 in depleting Wnk1 and Wnk2 protein. In contrast, a Sarm1 mutant that lacks the catalytic domain is not able to deplete Wnk1 or Wnk2 protein (Fig. 8H-I). While it is known that Nmnat can enzymatically increase NAD+ levels, it is unclear how Wnk proteins exert their role in axon protection. We found, however, that dWnk wild type function as well as its ability to suppress dSarm gain of function, depend on its kinase activity (**Fig. S15**).

Together these results suggest that the degeneration effector SARM1 is capable of downregulating WNK and NMNAT expression when co-expressed in cell culture. This *in vitro* result is consistent with our genetic epistasis experiments showing antagonistic relations between dWnk/Nmnat and dSarm.

DISCUSSION

In this study, we report that the function of the Wnk-family kinases (*Drosophila* dWnk and mammalian WNK1/2), are required in developmental axonal branch patterning as well as

axon maintenance. We show that phenotypic defects observed in mechanosensory axons of dWnk mutant neurons are indistinguishable from defects observed in Nmnat mutant neurons. Both dWnk and Nmnat mutant mechanosensory axons can grow from the periphery to the VNC but require dWnk as well as Nmnat function during axonal branch growth and patterning. Moreover, a post-developmental knock-down of dWnk triggered progressive degeneration in mature and fully developed mechanosensory axons. Such an adult-specific function is also analogous to the well-documented role of Nmnat in axon maintenance (Gilley and Coleman 2010; Wen et al. 2011; Ali et al. 2013; Sasaki et al. 2016). While Nmnat, has been studied most extensively for its role in axon maintenance in injury models or neurodegenerative disease models, it has been reported previously that LOF mutants are lethal and show axonal defects (Huppke et al. 2019; Lukacs et al. 2019). Furthermore, we show here that the dual developmental/maintenance functions of dWnk are evolutionary conserved as knock-down of WNK1 and WNK2 results in remarkably similar axon morphogenesis defects and trigger axon degeneration in mouse cortical neurons. We conclude, that in neurons Wnk kinases exert novel functions that are analogous and synergistic to conserved Nmnat functions. The discovery of Wnk kinases having important neuroprotective roles analogous to Nmnat offers new tools and insights to further dissect the complex regulatory network underlying active axon degeneration.

Formally, the adult maintenance defects that we observed upon Wnk depletion could be a consequence of developmental defects. However, several reasons argue strongly against this possibility: First, the *in vivo* knock-down of WNK1/WNK2 after postnatal day 30 in mouse cortical layer 2/3 PNs triggered degeneration of axons of mature neurons. Second, knock-down of dWnk at post-developmental (late pupal) stages does not alter the axonal branching or targeting of mechanosensory neurons, but triggered spontaneous degeneration of adult mechanosensory axons after 3 days post-eclosion. Third, a single copy RNAi knock-down of dWnk resulted in strong axon branching defects. Fourth, in previous studies, we identified and characterized several mutants that lead to severe axon branching defects of mechanosensory axons. For example, in Dscam1 null mutant clones the axon branching defects are even more severe than in dWnk mutant clones yet we found no sign of axon degeneration even in one week or older flies (see examples in (He et al. 2014; Dascenco et al. 2015). Fifth, even in cases of very short axon branches in dWnk or other mutants with a complete absence of contralateral projecting axon collaterals, the distal part of the mutant axons still reaches the corresponding ipsilateral target area. Given that putative trophic signals would have to support axons on both sides of the VNC, it seems highly unlikely that target derived trophic signals would only support contralateral projecting axon arbors. In summary, our data provide strong evidence that Wnk kinases have dual roles: first during

developmental axon morphogenesis, and second and independently, during continuous axon maintenance in mature neurons.

A key question raised by these results is: how similar are the molecular processes in developmental axon growth/branching and adult maintenance? A related question has been discussed in a hallmark review (Raff, Whitmore, and Finn 2002). This perspective article discussed the discovery that neurons can activate a self-destructive program independent of general apoptosis. The authors noted that neurons *"apparently have a second, molecularly distinct self-destruct program in their axon."* And the authors raise the incisive question: *"Do neurons also use this second program to prune their axonal tree during development and to conserve resources in response to chronic insults?"*

We assume that "pruning of axonal branches during development" could - as a cellular mechanism – also be involved in axonal branch patterning as analyzed here. Specifcally, we view the developmental axon branching of mechanosensory axons as a process where continuous competitive interactions among nascent branches select for stabilization or retraction (time scale minutes or few hours). In contrast, the well-characterized pruning of axons during metamorphosis (e.g. mushroom body remodeling) is initiated when axon branches and connectivity have been already established. This type of pruning (remodeling) requires primarily a destabilization of a fully established axon projection and is likely different from axonal branch selection as investigated here. Consistent with this idea is the finding that Nmnat is not required in axon pruning of mushroom body neurons (Hoopfer et al. 2006).

Our results now provide genetic and molecular data that support the notion that components of a "distinct self-destruct program" are involved in axon branch stabilization/destabilization. We further suggest that molecular control mechanisms of axon branching and axon destruction (or preventing axon destruction, i.e. axon maintenance) are mechanistically related. Specifically, the dynamics of axon branching requires the selection of an exuberant number of nascent axon branches by either stabilizing or destabilizing nascent branches (Lewis, Courchet, and Polleux 2013). During axon morphogenesis, the majority of filopodia/nascent branches are retracted to maintain just a few that are consolidated into axon collaterals. It seems plausible, therefore, that axon branch retraction in developing neurons might involve molecular effectors that are also required for a distinct type of axon branch pruning. Based on our *in vitro* studies we speculate that regulation of de novo protein synthesis could be the molecular process that is targeted in both, axon branching and axon maintenance.

Based on our new findings, we suggest that Wnk as well as Nmnat are necessary components of axon branching as well as axon maintenance. Support for this model comes from the results of our genetic epistasis analysis. The loss of d*Wnk* during axon branching

is only a problem if Sarm or Axed are present: in the absence of *Axed* (the most downstream effector of the destruction program in *Drosophila* known so far) (Neukomm et al. 2017), loss of dWnk does not cause defects in axonal branching or maintenance. Implicit to this model is that dWnk is unlikely instructing axon branching but rather provides a safeguard function curbing destructive effectors such that retraction, pruning, or branch destruction, can be restricted and constrained in a spatially restricted manner. A further implication of this model is the notion that loss of dWnk effectively represents a gain of function (on-switch) of an axonal destruction program in developing axons.
In this context it is also interesting to note that expression of Nmnat can compensate (i.e. rescue) for loss of dWnk in both axon branching and maintenance. It is well established that local depletion of Nmnat in adult neurons does directly lead to axon degeneration, i.e. has a role in axon maintenance independent of its developmental role (Milde, Gilley, and Coleman 2013). This is consistent with our new finding that post-developmental inactivation of dWnk or mammalian Wnk1/2 triggers axon degeneration.

Nmnat has been previously shown to protect from axon degeneration following axotomy by counter acting Sarm-induced NAD+ depletion (Essuman et al. 2017; Sasaki et al. 2016; Yang et al. 2015; Gerdts et al. 2015) and Axed activity (Neukomm et al. 2017). We show in the present study that even in the absence of axon injury, loss of Nmnat as well as loss of dWnk, or overexpression of dSarm and Axed lead to progressive degeneration of adult mechanosensory axons without injury. This is consistent with previous reports showing that Nmnat loss in sensory neurons of the wing lead to spontaneous axon degeneration in adult flies (Fang et al. 2012) or that loss of NMNAT2 leads to truncation of peripheral nerve and CNS axon tracts in mice (Gilley et al. 2013). A role of Wnk1 in axon maintenance is also consistent with the finding that WNK function has been linked to a severe form of peripheral neuropathy (Lafreniere et al. 2004; Rivière et al. 2004; Roddier et al. 2005; Coen et al. 2006).
Our results, therefore, support the notion that both axon morphogenesis and maintenance require a constitutive involvement of Wnk and Nmnat.
A link between dWnk, Nmnat and axon destructive factors is further corroborated by our biochemical experiments co-expressing these factors and using co-immunoprecipitations to analyze protein-protein interactions of dWnk or mammalian WNK1/2. First, our results suggest the possibility that dWnk, Nmnat, Sarm1, and Axed are able to form mixed complexes. Moreover, mammalian WNK1 can interact with WNK2 and Nmnat2 as well as SARM1. Although previous work has not identified Nmnat proteins as potential Wnk kinase substrates our results suggest that this possibility is worthwhile to examine in future experiments. Second, while a vertebrate orthologue of Axed has not been described, we

found that mammalian SARM1 overexpression strongly down-regulates levels of WNK1, WNK2, NMNAT2 and NMNAT1. While our cell culture experiments are supportive of such a possible Sarm1 function, future experiments will have to confirm that this downregulation of proteins by Sarm1 is also occurring in neurons *in vivo*.

It has been reported that inhibition of axon degeneration can be accomplished by increasing or stabilizing levels of Nmnat protein (Babetto et al. 2013). Moreover, Highwire/Phr1, which is an additional conserved factor functioning in Wallerian degeneration, directly promotes the downregulation of Nmnat and axon degeneration is strongly inhibited in Highwire/Phr1 mutants (Xiong et al. 2012). This previously described regulation of Nmnat levels is mediated via MAPK signaling and ubiquitin-dependent proteolysis. Our findings reported here suggest that Sarm1 may rather inhibit *de novo* protein synthesis in order to deplete Nmnat and other axon protective factors. Future studies will have to investigate in detail how the SARM1-dependent depletion of NAD+ also leads to a Wnk/Nmnat protein depletion as described here. Particularly interesting will be to determine how the destructive activity of Sarm protein can be limited during development to selective axon branch compartments in order to enable local axon branch pruning but prevent progressive axon degeneration.

Finally, Nmnat function has not only been involved in neuroprotection as a response to injury such as axotomy, but also in a diverse range of neurodegenerative diseases such as spinocerebellar ataxia (Zhai et al. 2008; Ruan et al. 2015), or FTD/Parkinsonism(Ali et al. 2013), or glaucomatous optic neuropathy (Munemasa and Kitaoka 2015), or following growth factor deprivation (Vohra et al. 2010). In future studies, it will be important to consider the possibility that the newly identified dWnk and WNK1/WNK2 kinases may also play similar neuroprotective roles in diverse types of neurodegenerative conditions.

Acknowledgement:

This work was supported by FWO (G077013N, G0B8919N) (DS), (G1214420N) (G. E-F.), VIB Belgium (DS), and the Humboldt Foundation (DS), the Fondation pour la Recherche Medicale (AJE20141031276) and ERC Starting Grant (678302-NEUROMET) (JC), NINDS NS107483 (FP), an award from the Roger De Spoelberch Fondation (FP) and an award from the Thompson Family Foundation Initiative (FP). This work was performed within the framework of the LABEX CORTEX (ANR-11-LABX-0042 / ANR-11-IDEX-0007). We thank our lab members for critical reading of the manuscript. Stocks obtained from the Bloomington Drosophila Stock Center (NIH P40OD018537) were used in this study. We thank M. Freeman, L. Neukomm, and T. Suzuki for sharing mutant fly stocks. We thank the personnel from the SCAR and ALECS-SPF mouse facility for animal care.

Author contributions:

A.I., J.C., F.P., and D.S. designed the experiments and wrote the manuscript. A.I., D.A., S.V., M.P., D.D., Y.K., J.Y., G.E-F., conducted the developmental and Drosophila genetics experiments. J.C., D.M.V, S.H., L.M., T.L., conducted the in vivo and in vitro mouse experiments. T.V., A.M., S.V., S.S., B.Y., M-L.E., J.Y., J.C. conducted molecular and cell culture work.

FIGURE LEGENDS

Figure 1. Loss of *Drosophila* dWnk results in axon branching defects in mechanosensory neurons. (A) Stereotyped branching pattern of *Drosophila* mechanosensory neurons. **(B-C)** GFP- labeled population of mechanosensory axons within the anterior part of the VNC. Note the complete lack of commissure (white arrows) in dWnk RNAi knock down. **(D-M)** Representative confocal images of mechanosensory neurons dye-filled with carbocyanine dyes. **(D** and **J)** WT pSc and pDc mechanosensory neurons displaying the stereotyped branching pattern. **(E-F** and **K)** dWnk RNAi and double RNAi ($RNAi^{2X}$) mediated knock-down defects results in branching defects. **(I)** Overexpression of dWnk can rescue branching defects in dWnk LOF. **(G-H** and **L-M)** dWnk LOF phenotypes using MARCM clones of two dWnk alleles, Wnk^{G1286} and Wnk^{F1183} also lead to defects in axon branch growth and patterning.

Figure 2. Loss of *Drosophila* dWnk function causes early onset neurodegeneration in mature sensory neurons and progressive loss of axons on thorax. (A) Schematic of *Drosophila* thorax showing the location of the scutellar mechaosensory neurons (in red) with a part of the proximal axon, cell body, dendrite (yellow box) and a distal axon in the ventral nerve cord (magenta box). **(B)** Magnified image of distal axon showing arborization of mechanosensory neurons. **(C)** A part of scutellum of adult *Drosophila* thorax (in gray) with anti-22C10 (microtubule binding protein) staining labeling of mechanosensory neuron (here pSc neurons). 22C10 labels microtubules in red and the CD8-GFP labeling axon membrane in green **(C** and **I-O)**. **(D-G)** Representative confocal images of mechanosensory neurons dye-filled with carbocyanine dyes. Loss of axon terminals in *Drosophila* mechanosensory neurons between 1 and 3 days in dWnk LOF. The axon degeneration in loss of dWnk knock down neurons starts at day 1 **(D)** followed by degeneration of distal axons **(E-F)**, and resulted in loss of axons in three days old samples **(G)**. **(H)** Quantification of the total number of degeneration processes in RNAi-mediated knock-down of dWnk (one copy and two copies and two different Wnk alleles ($WnkG^{1286}$ and $WnkF^{1183}$) at two developmental stages, one day and three days. **(I-O)** Process of axon degeneration in wild type **(I** and **M)** and dWnk homozygous mutant neurons using MARCM **(J-L** and **N)** in different developmental stages. **(J** and **L)** Genetic mosaic analysis shows that loss of dWnk leads to axon swelling and blebbing (arrows in magenta). Then, the axon starts to undergo fragmentation (arrow heads in magenta) **(K)**, followed by complete fragmentation and clearance of axonal debris **(N)**.

Figure 3. dWnk is required for developmental axon branching. (A) Schematic of a *Drosophila* mechanosensory neuron development. During early development, wild-type DC neurons growth cone enter the CNS at ~30 APF (after puparium formation) and undergo extensive expansion at ~32h APF **(A-B** and **C)**. During the intermediate phases, the growth cones composed of filopodia-like extension starting to expand and sprout into all directions at ~34h APF **(A** and **D)**. The number and length of filopodia is dramatically increased and segregated in opposite directions, along the anterior-posterior axis as well as toward the midline at ~36h APF **(A** and **E)**. In late development, the main axon shaft is growing in length and the midline projecting axon becomes more prominent and grows contralaterally ~38 hrs **(A** and **F)**. This process is sustained until the neurons reach their final length at ~ 40hrs APF, after which the axon matures and stabilizes its branching pattern **(A** and **G)**. **(H-M)** Growth cones of Dc neurons with dWnk double RNAi knockdown and Wnk LOF **(N-S)** are highly abnormal, exhibiting a reduced number of filopodia-like extensions. During the entire time course Wnk mutant axons are not capable of executing a normal axonal branching program. Even starting from the earliest time points of axonal sprouting (~30-32 hrs APF), the erroneous growth of axon collaterals, as well as strong deficits in spatial patterning of axon collaterals persists into later stages (~30-32 hrs APF) **(H-S). (T)** Quantification of the total number of filopodia at different developmental stages in control and Wnk mutant in animals of the genotypes indicated in panels B-M. The tests were considered significant when $p<0.05$, with the following criteria: * $p<0.05$, ** $p<0.01$, *** $p<0.001$, **** $p<0.0001$; ordinary one-way ANOVA with multiple comparisons.

Figure 4. Wnk1 and Wnk2 are both required for terminal axon branching and maintenance *in vivo*. (A-L) Representative images of the axons on the contralateral side of the electroporation in layer 2/3 PNs co-electroporated with tdTomato and control shRNA (A-D)**,** or *Wnk1* shRNA expressing (E-H) or *Wnk2* shRNA (I-L). *In utero* cortical electroporation (IUCE) were performed at E15 to electroporate neural progenitors generating layer 2/3 PNs and harvested at the following time points: P10 (immature), P15 (branching increasing), P21 (peak of branching) and P35 (adult pattern). Both *Wnk1* and *Wnk2* shRNA knockdown significantly reduce terminal branching of the callosal axons that reached the contralateral side and also reduce the total number of axons present at P35 (see also Fig. S9 for images of axons present at the midline at these time points). The numbers in the bottom left corner of each image correspond to the number of electroporated neurons on the ipsilateral side of each corresponding section. These neuron counts were performed using a machine-learning based segmentation tool (Ilastik – see Methods for details) and used to normalized the optical density measurements of tdTomato+ axons. (**M-P**) Optical density measurements of tdTomato+ axons on the contralateral side normalized by the number of electroporated

neurons on the ipsilateral side of each section. Three sections from each brain were quantified. $n_{pLKO\ P10}$=3; $n_{pLKO\ P15}$=3; $n_{pLKO\ P21}$=5; $n_{pLKO\ P35}$=5; $n_{WNK1\ P10}$=4; $n_{WNK1\ P15}$=3; $n_{WNK1\ P21}$=3; $n_{WNK1\ P35}$= 5; $n_{WNK2\ P10}$=3; $n_{WNK2\ P15=}$ 3; $n_{WNK2\ P21=}$4; $n_{WNK2\ P35=}$3. Statistical analysis: A two-way ANOVA followed by multiple Tukey's comparisons test: * p<0.05, ** p<0.01, *** p<0.001, **** p<0.0001. Scale bar in A-L: 100 microns.

Figure 5. *Wnk1* and *Wnk2* control axon branching and degeneration in cortical pyramidal neurons *in vitro.* (A-E) Representative cortical layer 2/3 pyramidal neurons imaged longitudinally at 5, 6, 7, 8, 9, and 10 DIV with only 5, 7, 9, and 10DIV ex utero electroporated with control shRNA (pLKO-scramble) (**A**), or with shRNA targeting *Wnk1* (**B** and **D**) or *Wnk2* (**C** and **E**). We distinguished two classes of neurons based on their phenotypes: neurons that showed clear signs of degeneration (axon blebbing and ultimately cell fragmentation) (panels **B** and **C**) and neurons that did not show any sign of degeneration at least during the 10DIV(**D** and **E**). Neuronal morphology was visualized by tdTomato expression and pseudo-colored to represent consecutive days of imaging. **(F)** Quantification of ultimate neuronal fate at 10DIV for the pLKO, shWNK1, and shWNK2 conditions as determined by the presence (degenerate) or absence (non-degenerate) of neuronal fragmentation. (**G-I**) Quantification of axonal arbor complexity and growth as measured by the total area occupied by the axon **(G** and **I)** of either non-degenerate **(G)** or degenerate **(I)** neurons and by the axon growth rate **(H** and **J)** as measured by the total area occupied by the axon cumulatively gained each day for both non-degenerate **(H)** and degenerate **(J)** neurons. Statistical analyses: Non-parametric Mann-Whitney test comparing each condition at each time point, with the data presented in **J-G** as mean and SEM. Number of neurons for quantification: n_{pLKO}=19, n_{shWNK1}=28, n_{shWNK2}=23 from at least three independent experiments. Significance: * p<0.05 with the following criteria: * p<0.05; ** p<0.01; ***p<0.001; ****p<0.0001. Scale bar in A-E: 100 microns.

Figure 6. Adult knockdown of *Wnk1* or *Wnk2* causes axonal degeneration in mouse cortical layer 2/3 pyramidal neurons. (A-B) Design of the conditional shRNA expression plasmids (CreON-shWNK) used to achieve inducible, adult knockdown of *wnk1* and *wnk2* in layer 2/3 PNs of the mouse cortex. Our strategy uses co-electroporation of a taxmoxifen-inducible form of Cre recombinase (ERT2-Cre-ERT2) in combination with a plasmid where a CMV enhancer/chicken-ß-Actin promoter (CAG) cassette flanked by incompatible Lox sites (Lox2272 and LoxP; subsequently referred to as FLEX plasmid) drives the expression of a fluorescent mStrawberry protein in absence of tamoxifen. In the presence of Tamoxifen, Cre is recombines the CAG promoter and flips its orientation to drive the expression of a mRNA

coding for EGFP and WNK shRNA (after 5' and 3' MiR processing). Our experimental design (B): at E15.5, mice undergo *in utero* electroporation with the CreON-shWNK plasmid and tamoxifen-dependent pCAG::ERT2-Cre-ERT2; at P30-P33, adult mice undergo four (one per day) consecutive intraperitoneal injections with tamoxifen diluted in corn oil (0.1 mg/g of bodyweight) or control vehicle only (corn oil); at P37 (8 days following first injection), mice were perfused, and their brains sectioned, immuno-amplified, and imaged. **(C-F)** Representative images of adult layer 2/3 PNs on ipsilateral side relative to *in utero* electroporated cortex of mice injected with vehicle **(C-D)** or with tamoxifen **(E-F)**. **(G-L)** Detail of a coronal brain section of a P37 mouse *in utero* co-electroporated with CreON-shWNK1 and ERT2CreERT2 showing **(H** and **K)** a reduction of callosal axonal projections and **(I, L)** a reduction in contralateral axonal branching upon adult knockdown of WNK1. Red inset numbers indicated the number of electroporated PNs, green inset numbers represent the number of EGFP+ PNs. **(M-N)** Quantification of RFP fluorescence (± SEM) in mice *in utero* electroporated with CreON-shWNK1 and ERT2CreERT2 along the radial axis of the cortical wall in the contralateral cortex **(M)** or corpus callosum **(N)** at P37 in mice previously injected with either vehicle or tamoxifen, normalized to the total number of electroporated cells.
(**P-U**) Representative coronal brain section of a P37 mouse *in utero* electroporated with CreON-shWNK2 and ERT2CreERT2 showing a reduction of callosal axonal projections (H and K) and a reduction in contralateral axonal branching upon adult knockdown of WNK2 (I and L). Red inset numbers indicated the number of electroporated PNs, green inset numbers represent the number of EGFP+ PNs. (**V-W**) Quantification of RFP fluorescence (± SEM) in mice *in utero* electroporated with CreON-shWNK2 and ERT2CreERT2 along the radial axis of the cortical wall in the contralateral cortex **(V)** or corpus callosum **(W)** at P37 in mice previously injected with either vehicle or tamoxifen, normalized to the total number of electroporated cells. Statistical analyses: Mann-Whitney test **(N** and **W)** or a two-way ANOVA followed by Tukey's multiple comparisons test (**M** and **V**): * $p<0.05$, ** $p<0.01$, *** $p<0.001$, **** $p<0.0001$. Number of mice for each experimental condition: $n_{CreON\text{-}shWNK1 + Vehicle} = 3$; $n_{CreON\text{-}shWNK1 + Tamoxifen} = 3$; $n_{CreON\text{-}shWNK2 + Vehicle}=3$, $n_{CreON\text{-}shWNK2 + Tamoxifen}=4$. At least 3 sections analyzed per brain as described for Figure 4. Scale bar in C-F: 150 microns; G-U: 100 microns.

Figure 7. Genetic epistatic analysis reveals that dWnk positively enhances Nmnat function and negatively regulates Axed and dSarm in the control of both axon branching and axon maintenance. (A-N) Representative confocal images of mechanosensory neurons dye-filled with carbocyanine dyes. **(A)** WT mechanosensory neurons displaying the stereotyped branching pattern. **(C-G)** dWnk loss of function (LOF), Nmnat LOF, Nmnat RNAi, Axed overexpression (GOF) and overexpression of dSarm are

showing very similar phenotype i.e. axon branching defects with loss of distal axon terminals. **(B, H** and **I)** overexpression of dWnk and Nmnat as well as Axed knock down are showing normal branching pattern. **(J-K)** dWnk LOF induced axon branching defects can be rescued by Axed RNAi-knockdown and overexpression of Nmnat which is showing normal branching pattern. **(L-N)** Overexpression of dWnk can maintain the axonal branches otherwise disrupted by Nmnat RNAi, Axed GOF and dSarm GOF. **(O)** Quantification of axonal branching defects observed in the various conditions described above. **(P-W)** Visualizing distal to proximal axon degeneration of mechanosensory neurons in thorax at day one and three. **(P** and **T)** Nmnat OE and Axed KD are showing a near continuous labeling of the microtubule cytoskeleton using anti-22C10 antibody staining same as wild type control samples **(Q** and **U)** Genetic mosaic analysis of Nmnat homozygous mutant mechanosensory neurons shows that lacking Nmnat leads to axon swelling and blebbing (arrows in magenta) in one day old samples followed by axon fragmentation and clearance of axonal debris (arrowheads in magenta) in three days old samples. **(R** and **V)** Overexpression of Nmnat can rescue the axon degeneration caused by loss of dWnk. **(S** and **W)** Knock-down of Axed prevent axon degeneration caused by dWnk LOF. **(X)** Quantification of axon degeneration in mechanosensory neuron proximal to the cell body located in thorax in the various conditions described for panels P-W'.

Figure 8. SARM1-dependent downregulation of Wnk and Nmnat. **(A)** dWnk interacts with dNmnat. dNmnat expression was induced using $CuSO_4$ in stable *Drosophila* S2 cells. Endogenous dWnk was precipitated using magnetic beads and co-precipitated protein complexes were analyzed using an HA-tag specific antibody. Non-coated beads were used as mock control. **(B)** The mammalian N-terminal domain of WNK1 interacts more stringently with mammalian NMNAT2 than its kinase domain. Validation of interactions by co-immunoprecipitation. HEK293T cells were co-transfected with rat WNK1 domains together with human HA-tagged NMNAT2. WNK1 domains were precipitated using anti-FLAG magnetic agarose. Co-precipitated protein complexes were analyzed by western blot (WB) using an HA-tag specific antibody. **(C)** Mammalian WNK1 and WNK2 are interacting. Validation of interaction by co-immunoprecipitation. SH-SY5Y cells were co- transfected with mammalian myc-tagged WNK1 and V5-tagged WNK2. WNK1 was precipitated using anti-myc magnetic beads and co-precipitated protein complexes were visualized by WB using a V5-tag specific antibody. **(D-G)** SARM1 NAD+ catalytic activity is required for regulation of WNK1, WNK2 and NMNAT2 expression. WB images and quantification of expression of myc-tagged WNK1 and WNK2-V5 **(D)**, NMNAT1-FLAG **(E)** and NMNAT2-FLAG **(F)** when co-transfected with either a GFP-containing plasmid or SARM1-HA. Graphs represent optical density measurements for indicated bands showing mean ± SEM of 2-4 independent

experiments **(G)**. α-Tubulin was used as loading control. **(H-I)** SARM1$^{\Delta TIR}$-HA does not reduce expression levels of myc-tagged WNK1 (H) and V5-tagged WNK2 (I) to the same extent as full-length SARM1-HA and SARM$^{\Delta ARM}$ mutants. For both WB, actin was used as a loading control.

STAR★METHODS

KEY RESOURCES TABLE

REAGENT or RESOURCE	SOURCE	IDENTIFIER
Antibodies		
Rabbit anti-GFP	Invitrogen	Cat# A-11122
Mouse anti-GFP	Abcam	Cat#ab1218
Rabbit anti-DsRed	Takara Bio	Cat#632496
Mouse anti-Fasciclin II (FasII) ID4	Developmental Studies Hybridoma Bank (DSHB)	RRID:AB_528235
Rat anti-N-Cadherin	Developmental Studies Hybridoma Bank (DSHB)	RRID:AB_528121
Guinea Pig anti-Wnk	This paper, Schmucker lab	N/A
Alexa Fluor 488 goat anti-rabbit IgG (H+L)	Invitrogen	Cat#A-11034
Alexa Fluor 488 goat anti-mouse IgG (H+L)	Invitrogen	Cat#A11029
Alexa Fluor 555 goat anti-rabbit IgG (H+L)	Invitrogen	Cat#A21429
Alexa Fluor 488 Goat anti-Guinea Pig IgG (H+L)	Invitrogen	Cat#A-11073
Alexa Fluor 647 Goat anti-Guinea Pig IgG (H+L)	Invitrogen	Cat#A-21450
Chicken polyclonal anti-GFP	Aves Lab	SKU: GFP-1020
Rabbit polyclonal anti-RFP	Abcam	Cat#: Ab124754
Rabbit polyclonal anti-CUX1 (M-222)	Santa Cruz	Cat#: Sc-13024
Rat anti-HA High Affinity	Roche	Cat#: 11867423001
Rabbit anti-p44/42 MAPK (Erk1/2)	Cell Signaling Technology	Cat#: 9102S
Alexa Fluor 488 Goat anti-Chicken IgY (H+L)	Invitrogen	Cat#: A-11039
Alexa Fluor 546 Goat anti-Rabbit IgG (H+L)	Invitrogen	Cat#: A-11010
Peroxidase AffiniPure Donkey Anti-Rabbit IgG (H+L)	Jackson ImmunoResearch	Cat# 711-035-152
Peroxidase AffiniPure Donkey Anti-Rat IgG (H+L)	Jackson ImmunoResearch	Cat# 712-035-153
Rabbit anti-FLAG	Sigma-Aldrich	Cat#: F7425
Mouse anti-V5	Sigma-Aldrich	Cat#: V8012
Rabbit anti-myc	Abcam	Cat#: ab9106
Rabbit anti-tubulin	Novus Biologicals	Cat#: NB600-936
Peroxidase AffiniPure Goat Anti-Rat IgG (H+L)	Jackson ImmunoResearch	Cat#: 12-035-003

Peroxidase AffiniPure Goat Anti-Rabbit IgG (H+L)	Jackson ImmunoResearch	Cat#: 111-035-144
Peroxidase AffiniPure Goat Anti-Mouse IgG (H+L)	Jackson ImmunoResearch	Cat#: 115-035-003
Peroxidase AffiniPure Goat Anti-Guinea Pig IgG (H+L)	Jackson ImmunoResearch	Cat#: 106-035-003
Chemicals, peptides, and recombinant proteins		
Fetal Bovine Serum	Gemini Bio-Products	Cat#100-500
B-27 Supplement (50x)	Fisher Scientific	Cat#A3582801
N-2 Supplement (100x)	Thermo Fisher Scientific	Cat#17502048
GlutaMAX™ Supplement	Thermo Fisher Scientific	Cat#35050061
Neurobasal Medium	Thermo Fisher Scientific	Cat#21103049
Hanks' Balance Salt Solution (HBSS), calcium, magnesium, no phenol red	Thermo Fisher Scientific	Cat#14-025-076
Penicillin/Streptomycin	Thermo Fischer Scientific	Cat#15140-122
Papain	Worthington	Cat#LK003178
DNase I	Sigma-Aldrich	Cat#D5025
Poly-d-Lysine	Thermo Fischer Scientific	Cat#A3890401
Fast Green FCF	Sigma-Aldrich	Cat#F7252-5G
DAPI Fluoromount-G	Southern Biotech	Cat#0100-20
32% Paraformaldehyde Aqueous Solution, EM Grade	Electron Microscopy Sciences	Cat#15614-S
Glutaraldehyde 25% Aqueous Solution	Electron Microscopy Sciences	Cat#16220
Tamoxifen, >99%	Sigma-Aldrich	Cat#T5648-1G
Corn Oil	Sigma-Aldrich	Cat#C8267-500ML
HOECHST 33258	Thermo scientific	Cat#62249
DiD	Invitrogen	Cat#D7757
DMEM/F-12	Gibco™	Cat#: 11320033
DMEM	Gibco™	Cat#: 11966025
Fetal Bovine Serum	Gibco™	Cat#: A4766801
Fetal Bovine Serum, heat inactivated	Gibco™	Cat#: 10082147
L-Glutamine	Gibco™	Cat#: 25030149
GENIUS DNA Transfection Reagent	Westburg	Cat#: WB 7-1050
Cycloheximide	Sigma-Aldrich	Cat#: C7698
Schneider's Insect Medium	Sigma-Aldrich	Cat#: S0146
Blasticidin	Invitrogen	Cat#: A1113903
Copper Sulfate	Sigma-Aldrich	Cat#: PHR1477
PBS	Gibco™	Cat#: 10010023
TWEEN® 20	Sigma-Aldrich	Cat#: 9005-64-5
Halt™ Protease and Phosphatase Inhibitor Cocktail (100X)	Thermo scientific	Cat#: 78440
Blotting-Grade Blocker	Biorad	Cat#: 1706404
Bovine Serum Albumin	Sigma-Aldrich	Cat#: A7030
Pierce™ ECL Western Blotting Substrate	Thermo scientific	Cat#: 32106
Pierce™ ECL Plus Western Blotting Substrate	Thermo scientific	Cat#: 32134
Pierce™ Anti-c-Myc Magnetic Beads	Thermo scientific	Cat#: 88842
Pierce™ Anti-HA Magnetic Beads	Thermo scientific	Cat#: 88837
Anti-V5-tag mAb-Magnetic Beads (Monoclonal Antibody)	MBL	Cat#: M167-11
In-Fusion HD Cloning Kit	Clontech	639649
Dynabeads™ Antibody Coupling kit	Invitrogen	Cat#: 14311D
Amaxa® Cell Line Nucleofector® Kit V	Lonza	Cat#: VCA-1003

Experimental models: Cell lines		
SH-SY5Y	ATCC	Cat#: CRL-2266
HEK293T	ATCC	Cat#: CRL-3216
S2	DGRC	stock #181
Experimental models: Organisms/strains		
Mouse F1 hybrid (C57BL/6J x 129/SvJ)	Mice, Polleux Lab, Charles River Labs	N/A; Strain Code: 027
UAS-Wnk RNAi	Drosophila stock Center Bloomington BDSC	RRID:BDSC_62150
UAS-Wnk RNAi	Drosophila stock Center Vienna VDRC	RRID:VDRCID_102654
pnr-Gal4	BDSC	RRID:BDSC_25758
Elav-Gal4	BDSC	RRID:BDSC_458
hsFLP, UAS-mCD8-GFP	BDSC	RRID:BDSC_28832
Wnk^{G1286}	(Berger et al. 2008)	N/A
Wnk^{F1183}	(Berger et al. 2008)	N/A
Wnk^{G1286} FRT80B	This paper	N/A
Wnk^{F1183} FRT80B	This paper	N/A
FRT80B Tub-Gal80	BDSC	RRID:BDSC_5191
UAS-Wnk^{WT}	This paper	N/A
FRT80B	BDSC	RRID:BDSC_1988
DC1.4-Flp	(Pfeiffer et al. 2008)	N/A
CantonS	BDSC	RRID:BDSC_64349
20xUAS-FRT- STOP-FRT-CD8GFP-2A-syt-mCherry	(Garrity et al. 1999)	N/A
UAS-NmnatRNAi	BDSC	RRID:BDSC_29402
$NMNAT^{2}$ FRT82B	(Neukomm et al. 2017), Freeman lab	N/A
FRT82B	BDSC	RRID:BDSC_2035
5xUAS-$axed^{long}$	(Neukomm et al. 2017), Freeman lab	N/A
5xUAS-$dSarm^{WT}$	(Neukomm et al. 2017), Freeman lab	N/A
UAS-Nmnat-HA	BDSC	RRID:BDSC_39702
UAS-Axed RNAi	BDSC	RRID:BDSC_58220
455-Gal4	(Hinz, Giebel, and Campos-Ortega 1994)	N/A
R15E08-Gal4	(Pfeiffer et al. 2008)	N/A
UAS-Wnk-EYFP	This paper	N/A
P{QUAS-mCD8-GFP.P}5J	BDSC	RRID:BDSC_30003
Gr21a-GAL4.C	BDSC	RRID:BDSC_23890
Or88a-GAL4.F	BDSC	RRID:BDSC_23137
ato-Gal4-14a	(Srahna et al. 2006), Hassan lab	N/A

ato-Gal4.3.6-10	(Srahna et al. 2006), Hassan lab	N/A
hsFLP, tubP-GAL80, FRT19A	BDSC	RRID:BDSC_5134
FRT19A	BDSC	RRID:BDSC_1744
UAS-Fray RNAi	BDSC	RRID:BDSC_42569
UAS-Kcc RNAi	BDSC	RRID:BDSC_34584
UAS-dSarm RNAi	BDSC	RRID:BDSC_31175
UAS-Wnk$^{kinase\ dead}$	This paper	N/A
Recombinant DNA		
Plasmid: pCAG-TdTomato	(Lewis et al. 2016)	N/A
Plasmid: pLKO.1	The RNAi Consortium shRNA Library; OpenBioSystems	Cat#UN3245
Plasmid: pLKO-shWNK1-TRC0000027035	The RNAi Consortium shRNA Library; OpenBioSystems	RMM3981-201757342
Plasmid: pLKO-shWNK1-TRC0000027039	The RNAi Consortium shRNA Library; OpenBioSystems	RMM3981-201757346
Plasmid: pLKO-shWNK2-TRC0000027606	The RNAi Consortium shRNA Library; OpenBioSystems	RMM3981-201757913
Plasmid: pLKO-shWNK2-TRC0000027661	The RNAi Consortium shRNA Library; OpenBioSystems	RMM3981-201757968
Plasmid: pLKO-shWNK2-TRC0000027668	The RNAi Consortium shRNA Library; OpenBioSystems	RMM3981-201757975
Plasmid: pCAG-CreON-WNK1-27035	This paper	N/A
Plasmid: pCAG-CreON-WNK1-27039	This paper	N/A
Plasmid: pCAG-CreON-WNK2-27661	This paper	N/A
Plasmid: pCAG-CreON-WNK2-27668	This paper	N/A
Plasmid: pCAG-ERT2CreERT2	(Matsuda and Cepko 2007)	Addgene Plasmid #13777
Plasmid: pCIG2-HA-WNK1	This paper	N/A
Plasmid: pSCV2 (pCAG-mVenus)	(Hand and Polleux 2011)	N/A
Plasmid: pCMV-myc-WNK1	(Xu et al. 2000)	Addgene Plasmid #38779
Plasmid: pCDNA3-WNK2-V5	(Chen et al. 2011)	Addgene Plasmid #24569
Plasmid: pUASattB-dWnk	This paper	N/A
Plasmid: pUASattB-Axed	This paper	N/A
Plasmid: pMT-V5-Axed	This paper	N/A
Plasmid: pCDNA5-NMNAT1-EYFP-FLAG	This paper	N/A
Plasmid: pCDNA5-NMNAT2-EYFP-FLAG	This paper	N/A
Plasmid: pCDNA5-SARM1-ECFP-HA	This paper	N/A
Plasmid: pCDNA5-SARM1-ΔTIR-ECFP-HA	This paper	N/A
Plasmid: pCDNA5-turboGFP	This paper	N/A
Plasmid: pCMV-FLAG-NMNAT2	(Gilley and Coleman 2010)	N/A

Plasmid: pCMV-FLAG-WldS	(Gilley and Coleman 2010)	N/A
Software and algorithms		
Ilastik: density counter	(Berg et al. 2019)	https://www.ilastik.org/
FIJI is a modified ImageJ distribution	(Schneider, Rasband, and Eliceiri 2012)	https://imagej.nih.gov/ij/
GraphPad PRISM	GraphPad Software Inc.	https://www.graphpad.com/scientific-software/prism/
NIS-Elements	Nikon	https://www.microscope.healthcare.nikon.com/products/software/nis-elements
A1R Confocal Microscope	Nikon	https://www.microscope.healthcare.nikon.com/products/confocal-microscopes/a1hd25-a1rhd25
LSM 710 confocal microscope	Zeiss	https://www.zeiss.com/microscopy/int/products/confocal-microscopes.html
LSM 780 confocal microscope	Zeiss	https://www.zeiss.com/microscopy/int/products/confocal-microscopes.html
ProteinSimple FluorChemQ imaging system	ProteinSimple	https://www.proteinsimple.com/fluorchem_m.html
Chemi-Doc_IT imager	UVP	https://www.uvp.com/products/

RESOURCE AVAILABILITY

Lead contact

- Further information and requests for resources and reagents may be directed to and will be fulfilled by the Lead Contact, Dr. Dietmar Schmucker (dslab@uni-bonn.de).

Materials availability

- Fly strains and expression constructs generated in this study are available from the Lead Contact upon request. Plasmids can be obtained with a completed Materials Transfer Agreement as requested by Flanders Institute of Biotechnology (VIB).

Data and code availability

- All relevant data supporting the findings of this study are listed in Key Resource Table or are available from the Lead Contact upon request.
- This paper does not report original code
- Any additional information required to reanalyze the data reported in this paper is available from the lead contact upon request.

EXPERIMENTAL MODEL AND SUBJECT DETAILS

Flies (*D. melanogaster*) genotypes for all experiments and all figure panels are listed in Table S1. For all genetic crosses males and female flies were used. UAS-RNAi lines were obtained from the Vienna *Drosophila* Resource Center (Vienna, Austria) or from the Bloomington *Drosophila* stock center (Indiana University, USA). All crosses were performed at 25°C, except for late knock-down of dWnk, for which a shift from 18°C to 29°C at late-pupal stage (after axon branching had already occurred) was used to prevent RNAi activation during development, and the presence of normal axon morphologies was confirmed in young adult control flies. Single-cell labeling and transgene expression were performed as described (Urwyler et al. 2019). For analysis of axon branch patterns of dye-labeled mechanosensory neurons at adult stages only VNCs of female animals were used in order to avoid variability due to size differences of male and female flies. In all other experiments male and female animals were used.

Mice were used according to protocols approved by the Institutional Animal Care and Use Committee at Columbia University Medical School and the Ethics committee of the University of Lyon, and in accordance with National Institutes of Health guidelines and the French and European Union legislation. All animals were maintained in a 12-hour light/dark cycle. We crossed C57BL/6J males with 129/SvJ females to generate F1 hybrids (C57BL/6J x 129/SvJ). Time-pregnant F1 hybrid females were obtained by overnight breeding with C57BL/6J males. Noon following breeding was considered E0.5. Embryos of both sexes

were used in electroporation procedures. Electroporations were performed at developmental stage E15.5. Mice were sacrificed at the age indicated in the figures.

METHOD DETAILS

Plasmids and molecular cloning

Empty vector pLKO.1 and shRNA targeting plasmids toward mouse WNK1 (TRC0000027035 and TRC0000027039) or mouse WNK2 (TRC0000027606, TRC0000027661 and TRC0000027668) were selected from The RNAi Consortium shRNA Library (TRC) from the Broad Institute and purchased from OpenBioSystems. Unless stated otherwise shRNA plasmids targeting a same gene were pooled at a 1:1 (WNK1) or 1:1:1 (WNK2) ratio and used at the final concentration of 1 mg/mL for *in utero* cortical electroporation or *ex vivo* electroporation. The CreON-shWNK plasmids were synthesized (Vigene) using these same shRNA targeting sequences under a CMV promoter. The CMV promoter was then replaced with a CMV enhancer/chicken β-Actin promoter (CAG) sing PCR amplification and InFusion cloning (Clonetech). pCAG-ERT2CreERT2 has been described previously (Matsuda and Cepko 2007) and was purchased via Addgene (Addgene #13777).

Plasmids containing rat myc-WNK1, human WNK2-V5, and mouse SARM1 were a gift from Melanie Cobb, Joseph Costello, and Yi-Ping Hsueh, respectively (Addgene plasmid #38779, #24569, and #50707) (Xu et al. 2000; Chen et al. 2011; Hong et al. 2007). The mVenus expressing vector pSCV2 was described previously (Hand and Polleux 2011). Human NMNAT1 and NMNAT2 were PCR amplified from clone HsCD00353283 and HsCD00399665 from the DNASU plasmid repository. dWnk and Axed were amplified from *Drosophila* cDNA and cloned into pUASTattB using Gibson Assembly (NEB E2611S). In order to create a stable *Drosophila* cell line, Axed was additionally subcloned into pMT-V5-His A (Thermo Scientific) using Gibson Assembly, and pCoBlast (Thermo Scientific) was used as a selection vector. All expression vectors used for cell line transfections were further constructed using the Gateway cloning system (Life Technologies). In brief, NMNAT1, NMNAT2, and SARM1 open reading frames were amplified by PCR adding a 5' attB1 site and a mammalian Kozak sequence in the forward primer, as well as a 3' attB2 sequence in the reverse primer. SARM1ΔTIR was generated by amplifying solely the N-terminal SARM1, excluding the 165 amino acids at the C-terminal comprising the TIR (Toll/Interleukin-1 Receptor) domain. The stop codon was removed to allow in-frame C-terminal tagging. In a similar manner, turboGFP (GFP) was amplified with the retention of the stop codon to use as a transfection control. The amplicons were subcloned into a modified version of pDONR223 (Rual et al. 2004) by a BP transferase reaction. Subsequently, an LR reaction was performed according to the manufacturer's instructions with pcDNA5FRT-TO-GW-EYFP-

FLAG and pcDNA5FRT-TO-GW-ECFP-HA destination vectors to generate NMNAT1-EYFP-FLAG, NMNAT2-EYFP-FLAG, SARM1-ECFP-HA, and SARM1ΔTIR -ECFP-HA. Finally, pCMV-FLAG-NMNAT2 and pCMV-FLAG-WldS were a gift of the Coleman lab.

Cell cultures and transfections

Primary neuronal cultures were performed as described previously (Polleux and Ghosh 2002). Mouse cortices were dissected in Hank's Buffered Salt Solution (HBSS) supplemented with 2.5 mM Hepes, 1 mM $CaCl_2$ (Sigma), 1 mM $MgSO_4$ (Sigma), 4 mM $NaHCO_3$ (Sigma) and 30 mM D-glucose (Sigma), hereafter referred to as cHBSS. Cortices were dissociated in cHBSS containing papain (Worthington) and DNAse I (100 µg/mL, Sigma) for 20 min at 37°C, washed three times and manually triturated in cHBSS supplemented with DNAse. Cells were then plated at 7.5 x 10^4 cells per 35 mm glass bottom dish (Matek) coated with 1 mg/mL poly-D-lysine (Sigma) and cultured for 5, 10, 15 or 20 days in Neurobasal medium supplemented with 1x B27, 1x N2, 2 mM L-glutamine and 5 units/mL penicillin- 50 mg/mL streptomycin.

SH-SY5Y cells (ATCC, CRL-2266) and HEK293T cells (ATCC, CRL-3216) were cultured in DMEM/F12 and DMEM, respectively, supplemented with 10% FBS, 2 mM L-Glutamine and 100 units/mL penicillin- 100 µg/mL streptomycin. Cell transfection were performed in 6-well plates using GENIUS DNA transfection reagent with 2 µg of each plasmid. Unless otherwise indicated, all products for cell cultures were obtained from Invitrogen/Life Technologies. For cycloheximide (CHX) experiments, HEK293T cells were treated with the inhibitor at 100 µg/mL starting 24 hours after transfection. Protein lysates were prepared at t = 0 (no CHX treatment) and at 2, 4 and 6 hours of CHX treatment.

Drosophila S2 cells were obtained from DGRC and grown in Schneiders medium supplemented with 10% HI FBS and 100 units/mL penicillin- 100 µg/mL streptomycin (Invitrogen/Life Technologies). The stable cell line expressing Axed-V5 was grown in the presence of blasticidin (Life Technologies). Expression was induced using 500 µM $CuSO_4$. Cells were transfected using the Amaxa Nucleofector II device (Lonza) with 1 to 2 µg of DNA (solution V, program D023).

***Ex utero* and *in utero* cortical electroporations**

Ex utero electroporation of mouse dorsal telencephalic progenitors was performed as previously described (Courchet et al. 2013) by injecting plasmid DNA (1-2 µg/µL endotoxin-free plasmid DNA, Midi prep kit from Macherey-Nagel) plus 0.5% Fast Green (1:20 ratio, Sigma) using the picospritzer III (Parker) microinjector into the lateral ventricles of isolated E15.5 embryonic heads that were decapitated and placed in complete HBSS (Polleux and Ghosh 2002). Electroporations were performed on the whole head (skin and skull intact) with

gold-coated electrodes (GenePads 5 × 7 mm BTX) using an ECM 830 electroporator (BTX) and the following parameters: five 100 ms long pulses separated by 100 ms long intervals at 20 V. Immediately after electroporation, cortices were prepared for primary neuronal culture.
Protocol for *in utero* electroporation is fully described in (Meyer-Dilhet and Courchet 2020). We used timed-pregnant F1 females from C57BL/6J X 129/SvJ crosses (The Jackson Laboratory). Electroporation was performed at E15.5 to target progenitors generating cortical layer 2/3 PNs. The electroporation settings were: 4 pulses of 45 V for 50 ms with 500 ms interval. Electroporated mice were sacrificed at the indicated ages.

Immunoprecipitations

Immunoprecipitations were performed as described before (Sachse et al. 2019). Briefly, SH-SY5Y or HEK293T cells were harvested 24 to 48 hours after transfections in ice-cold 1x PBS and lysed in RIPA buffer (25 mM Tris pH 7.6, 150 mM NaCl, 1% sodiumdeoxycholate, 0.5% NP-40, 1% SDS, 0.5% Triton-X100, 5% glycerol) containing Halt protease and phosphatase inhibitor cocktail (Pierce). Input extracts were cleared by centrifugation and tagged proteins were precipitated for one hour at RT followed by extensive washing in RIPA buffer or TBS-Tween. For immunoprecipitation, we used the following magnetic beads: mouse anti-c-myc, mouse anti-HA (both Pierce), and mouse anti-HA (MBL). Following precipitations, protein complexes were heat-eluted in SDS sample buffer or 0.1M glycine.
Immunoprecipitation in S2 cells was performed 48 hours after the induction of the stable S2 cell line expressing Axed-V5. Induction was carried out 6 or 24 hours after transfection with the plasmid containing dWnk. Cells were harvested in RIPA buffer supplemented with protease and phosphatase inhibitors and proteins were precipitated for two hours at RT. The The Dynabeads™ Antibody Coupling kit (Invitrogen) was used to coat 3 mg beads with the custom-made dWnk antibody. 1 mg beads were used for the mock IP. Coupling of the antibody to the beads was carried out at 37 °C overnight.

Western blotting

Denaturated protein samples were submitted to SDS-PAGE and transferred to polyvinylidene difluoride (PVDF) or nitrocellulose membranes (Biorad). Primary antibody incubation was performed overnight at 4°C using the appropriate antibody diluted in TBS-Tween (0.1%) containing 5% milk or BSA. HRP-conjugated secondary antibodies were incubated at room temperature for 1 to 2 hours in in TBS-Tween with milk or BSA. Protein bands were visualized with a ProteinSimple FluorChemQ imaging system or Chemi-Doc_IT imager (UVP) using ECL reagent (Pierce). Three or more independent experiments were performed for all immunoblotting data.

Dye labelling of *Drosophila* mechanosensory neuron axons

Dye fills were performed as described previously (Chen et al. 2006). Adult flies were glued to an insect pin (Fine Science Tools, #26000-25) and large mechanosensory bristles on the dorsal thorax were plucked manually with forceps. Flies were subsequently beheaded, their abdomen opened and fixed overnight at 4 ºC in 3.7% (w/v) paraformaldehyde (Electron Microscopy Sciences) in 0.2 M sodium carbonate-bicarbonate ("carb-bicarb") buffer. After washes in 0.2 M carb-bicarb, flies were briefly dried and the lipophilic fluorescent dyes DiD (20 mg/mL in 100% ethanol, ThermoFisher, #D7757) and DiI (20 mg/mL in 1:1 dimethyl formamide:ethanol, ThermoFisher, #D3911) were applied to the exposed bristle sockets with glass micropipettes (Sutter Instruments, #BF100-50-10). Flies were incubated 48 hours in a humid chamber at room temperature, the ventral nerve cords (VNCs) were dissected in 0.2 M carb-bicarb buffer and filled mechanosensory axons were imaged on an LSM710 and LSM780 (Zeiss) confocal microscopes.

Labeling and analysis of growth cones of mechanosensory neurons during development

Genetic labeling of single pDc neurons was adapted from a genetic labeling strategy to investigate the developmental mechanism by which Wnk regulate axonal branch formation. Briefly, Flp-recombinase was expressed in precursors of pDc neurons using DC1.4 enhancer, which gives rise to stochastic expression. In this flp-out setups, pnr-gal4 activity was restricted

by using DC1.4-Flp to excise an FRT-flanked transcriptional STOP cassette from a UAS-mCD8::GFP reporter construct, whose expression is then trans-activated by pnr-Gal4. The defective branching pattern of adult pDc neurons with dWnk double RNAi knock-down is fully penetrant (n=47). The phenotypic defect(s) of the adult mutant pDc axon projection is identical to single pDc axons of dWnk-null mutant clones (generated by MARCM). White pupae were allowed to develop for various time intervals at 25°C until ~30 to 40 hr for wild type and dWnk-knockdown. Dissected VNCs were stained with anti-GFP. Images were taken on a Zeiss LSM710 confocal microscope with a 60X lens. Filopodia were counted manually in Fiji / ImageJ in confocal microscopy image stacks of developing dWnk-knockdown and control animals with single mechanosensory neurons labelled with CD8::GFP.

Conditional knockdown of WNK

E15.5 embryos of time-pregnant F1 females from C57BL/6J x 120/SvJ were *in utero* electroporated with pCAG-ERT2CreERT2 (1 mg/mL) and a 1:1 ratio of either CreONWNK1-TRCN0000027035 and CreONWNK1-TRCN0000027039 or CreONWNK2-

TRCN0000027661 and CreONWNK1-TRCN0000027668 (4 mg/mL). Activation of the ERT2CreERT2 fusion protein was achieved by intraperitoneal administration of tamoxifen for three consecutive days, starting at P30, (0.10 mg/g of bodyweight) dissolved in corn oil (20 mg/mL) as previously described (Matsuda and Cepko, 2007). Corn oil alone was used as a vehicle control for littermates. Four days after the last injection i.e. 7 days following first injection (P37), mice were sacrificed via perfusion of 4% paraformaldehyde (PFA, Electron Microscopy Sciences) and 0.075% Glutaraldehyde (Electron Microscopy Sciences) followed by overnight post-fixation in 4% PFA/0.075% Glutaraldehyde.

Immunohistochemistry of Brain Slices

Post-fixed brains were sectioned via vibratome (Leica VT1200) at 110µm. Floating sections were then incubated for 1 hour in 4% Normal Goat Serum, 2% BSA, 0.3% Triton X-100 in PBS to block non-specific binding. Primary and secondary antibodies were diluted as follows: chicken anti-GFP (5 µg/mL, Aves Lab-recognizes GFP and YFP; rabbit anti-RFP (1:1,000, Abcam–recognizes mTagBFP2, DsRED, and tdTomato); AlexaFluor goat anti-Chicken 488 (1:1000, Invitrogen); AlexaFluor goat anti-Rabbit 546 (1:1,000, Invitrogen). Floating sections were incubated overnight at 4ºC in the primary antibodies, washed three times in PBS for 5 minutes each, then incubated in secondary antibodies for 5 hours at room temperature. Sections were mounted on slides and cover slipped with Fluoromount-G mounting medium
(SouthernBiotech).

Immunolabelling

Cells were fixed for 5 min at room temperature in 4% (w/v) paraformaldehyde (Electron Microscopy Sciences) in PBS. Fixed cells were subsequently incubated in Permeabilisation Buffer (PB) (1x PBS supplemented with 0.1% Triton-X100 and 1% BSA (Sigma)) for 60 minutes to permeabilize and block non-specific staining. Primary antibodies were incubated for 1 hour at room temperature in PB, followed by an incubation with secondary antibodies for 30 min at room temperature in PB. Coverslips were mounted on slides with Vectashield mounting medium.

Drosophila single mechanosensory neuron labelling with axon and synaptic markers was done as described previously (Chen et al. 2006).

Mice were anaesthetized with isofluorane before intracardiac perfusion with 4% (w/v) paraformaldehyde in PBS followed by post-fixation in 4% PFA for 2 hours. 125 µm coronal brain sections were obtained using a vibrating microtome (Leica VT1200S). Sections were permeabilized 30 minutes in PB then incubated overnight with the indicated primary antibodies diluted in PB. Secondary antibodies were incubated for 1 hour at room

temperature in PB. Slices were mounted on microscopy slides using Vectashield mounting medium.

Antibodies

The dWnk antibody was custom developed. For dWnk protein production in bacteria, PCR products of N-terminal and C-terminal fragments (as indicated in Fig. S2) were amplified and cloned into pET vectors. Protein fragments expressed from these plasmids were tagged with 6xHis. Constructs were transformed into BL21DE3 competent cells (Agilent, #200131). Expression was induced in liquid LB medium cultures by adding IPTG (Sigma, #I6758-1G). Cells were grown for another 3 to 4 hours at 25 ºC and subsequently lysed in lysis buffer containing 50 mM Tris-HCl (pH 7.5), 150 mM NaCl and 2 mM DTT with sonication. His-tagged proteins in the lysate were purified by use of Ni-NTA agarose beads (Qiagen, #30210) and

washed in 30 mM imidazole in lysis buffer. Protein was eluted with 300 mM imidazole in lysis buffer. The eluate was further purified on an Amicon Ultra 0.5 mL 3K UFC column (#500396). Purified proteins were used for immunization of guinea pigs. Polyclonal antibody production was done by Covance (Denver, PA, USA). The dWnk antibody was used at a 1:300 dilution.

Other primary antibodies used in this study were: chicken anti-GFP (5 µg/mL, Aves Lab), mouse anti-SMI312R (1:1000, Covance), rabbit anti-MAP2 (1:1000, Millipore), rabbit anti-Cux1 (1:500, Santa Cruz), rat anti-HA high affinity (1:1000, Roche), rabbit anti-FLAG (1:2500, Sigma), mouse anti-V5 (1:1000, Sigma), rabbit anti-myc (1:1000, Abcam), rabbit anti-tubulin (1:1000, Novus Biologicals), rabbit anti-GFP (Invitrogen, 1:500), mouse anti-GFP (Abcam, 1:500), rabbit anti-DsRed (Takara Bio, 1:500), mouse anti-Fasciclin II (DSHB Hybridoma Product 1D4 anti-Fasciclin II, 1:20), and rat anti-N-Cadherin (DSHB Hybridoma Product DN-Ex #8, 1:20). Alexa-conjugated secondary antibodies (Invitrogen) were used at a 1:2000 dilution. HRP-conjugated secondary antibodies (Invitrogen or Jackson Laboratories) were used at a 1:10000 dilution. Nuclear DNA was stained using Hoechst 33258 (1:10000, Pierce).

Confocal image acquisition and analysis

Confocal images were acquired with a Nikon Ti-E microscope equipped with the A1 laser scanning confocal microscope using the Nikon software NIS-Elements (Nikon Corporation, Melville, NY). Dye-filled *Drosophila* axons were imaged using an LSM710 (Zeiss) confocal microscope. Analysis of confocal images was performed with NIS-Elements software or ImageJ.

Ilastik Cell Density Counter

The interactive density counter workflow from open-source software, Ilastik (Berg et al. 2019), was used to quantify the number of layer 2/3 PNs electroporated in each brain section quantified for axon optical density in **Figures 4** and **6**. This workflow is useful for identifying overlapping objects that classic segmentation and detection approaches cannot separate. The counter employs a supervised learning strategy guided by user annotations of background and object, which then serve as inputs into a Random Forrest regression that estimates every pixel's density. 10x confocal images from four different brain slices that spanned all time points were used for training the algorythm. Post processing of our Ilastik density outputs were performed in FIJI ImageJ. This included binarizing and watershedding images. To count cells we employed FIJI's analyze particles function, excluding small objects and objects with low sphericity to remove objects corresponding to dendrite branches. To validate our Ilastik workflow we compared the cell count to manual counts performed by multiple observers (three). The number of cells per image estimated by Ilastik and Fiji pipeline lied within 10% of values obtained by human observers in a manner that was independent of density of electroporated neurons.

QUANTIFICATION AND STATISTICAL ANALYSIS

Data acquisition and quantification were performed non-blinded. Acquisition was performed in Microsoft Excel, statistical analyses were performed using Prism (GraphPad Software). Statistical details (definition of test, exact value of n (e.g., number of *Drosophila* VNCs, number of mouse brains, etc.), mean ± deviations, p values) are listed in Figure Legends and below.

Figure 3T: Ordinary one-way ANOVA with multiple Tukey's comparisons test, $n_{WT\text{-}early}$=16; $n_{WnkKD\text{-}early}$=13; $n_{WT\text{-}intermediate}$=17; $n_{WnkKD\text{-}intermediate}$=12; $n_{WT\text{-}late}$=14; $n_{WnkKD\text{-}late}$=10. The tests were considered significant when $p<0.05$, with the following criteria: * $p<0.05$, ** $p<0.01$, *** $p<0.001$, **** $p<0.0001$.

Figure 4M-P: Two-way ANOVA followed by multiple Tukey's comparisons test. Three sections from each brain were quantified, $n_{pLKO\ P10}$=3; $n_{pLKO\ P15}$=3; $n_{pLKO\ P21}$=5; $n_{pLKO\ P35}$=5; $n_{WNK1\ P10}$=4; $n_{WNK1\ P15}$=3; $n_{WNK1\ P21}$=3; $n_{WNK1\ P35}$= 5; $n_{WNK2\ P10}$=3; $n_{WNK2\ P15=}$ 3; $n_{WNK2\ P21=}$4; $n_{WNK2\ P35=}$3. Statistical analysis: * $p<0.05$, ** $p<0.01$, *** $p<0.001$, **** $p<0.0001$.

Figure 5G-J: Two-way ANOVA followed by multiple Tukey's comparisons test. Number of neurons for quantification: n_{pLKO}=19, n_{shWNK1}=28, n_{shWNK2}=23 from at least three independent

experiments. Significance: * p<0.05 with the following criteria: * p<0.05; ** p<0.01; ***p<0.001; ****p<0.0001.

Figure 6: Mann-Whitney test **(N** and **W)** or a two-way ANOVA followed by Tukey's multiple comparisons test (**M** and **V**): * p<0.05, ** p<0.01, *** p<0.001, **** p<0.0001. Number of mice for each experimental condition: $n_{CreON\text{-}shWNK1 + Vehicle} = 3$; $n_{CreON\text{-}shWNK1 + Tamoxifen} = 3$; $n_{CreON\text{-}shWNK2 + Vehicle}=3$, $n_{CreON\text{-}shWNK2 + Tamoxifen}=4$. At least 3 sections analyzed per brain as described for Figure 4.

DECLARATION OF INTEREST

The authors declare no competing interests.

REFERENCES

Alessi, D. R., J. Zhang, A. Khanna, T. Hochdörfer, Y. Shang, and K. T. Kahle. 2014. "The WNK-SPAK/OSR1 pathway: master regulator of cation-chloride cotransporters." *Sci Signal* 7 (334):re3. doi: 10.1126/scisignal.2005365.

Ali, Y. O., H. M. Allen, L. Yu, D. Li-Kroeger, D. Bakhshizadehmahmoudi, A. Hatcher, C. McCabe, J. Xu, N. Bjorklund, G. Taglialatela, D. A. Bennett, P. L. De Jager, J. M. Shulman, H. J. Bellen, and H. C. Lu. 2016. "NMNAT2:HSP90 Complex Mediates Proteostasis in Proteinopathies." *PLoS Biol* 14 (6):e1002472. doi: 10.1371/journal.pbio.1002472.

Ali, Y. O., D. Li-Kroeger, H. J. Bellen, R. G. Zhai, and H. C. Lu. 2013. "NMNATs, evolutionarily conserved neuronal maintenance factors." *Trends Neurosci* 36 (11):632-40. doi: 10.1016/j.tins.2013.07.002.

Anselmo, A. N., S. Earnest, W. Chen, Y. C. Juang, S. C. Kim, Y. Zhao, and M. H. Cobb. 2006. "WNK1 and OSR1 regulate the Na+, K+, 2Cl- cotransporter in HeLa cells." *Proc Natl Acad Sci U S A* 103 (29):10883-8. doi: 10.1073/pnas.0604607103.

Babetto, E., B. Beirowski, E. V. Russler, J. Milbrandt, and A. DiAntonio. 2013. "The Phr1 ubiquitin ligase promotes injury-induced axon self-destruction." *Cell Rep* 3 (5):1422-9. doi: 10.1016/j.celrep.2013.04.013.

Berg, S., D. Kutra, T. Kroeger, C. N. Straehle, B. X. Kausler, C. Haubold, M. Schiegg, J. Ales, T. Beier, M. Rudy, K. Eren, J. I. Cervantes, B. Xu, F. Beuttenmueller, A. Wolny, C. Zhang, U. Koethe, F. A. Hamprecht, and A. Kreshuk. 2019. "ilastik: interactive machine learning for (bio)image analysis." *Nat Methods* 16 (12):1226-1232. doi: 10.1038/s41592-019-0582-9.

Berger, J., K. A. Senti, G. Senti, T. P. Newsome, B. Asling, B. J. Dickson, and T. Suzuki. 2008. "Systematic identification of genes that regulate neuronal wiring in the Drosophila visual system." *PLoS Genet* 4 (5):e1000085. doi: 10.1371/journal.pgen.1000085.

Chen, B. E., M. Kondo, A. Garnier, F. L. Watson, R. Püettmann-Holgado, D. R. Lamar, and D. Schmucker. 2006. "The molecular diversity of Dscam is functionally required for neuronal wiring specificity in Drosophila." *Cell* 125 (3):607-20. doi: 10.1016/j.cell.2006.03.034.

Chen, C. Y., C. W. Lin, C. Y. Chang, S. T. Jiang, and Y. P. Hsueh. 2011. "Sarm1, a negative regulator of innate immunity, interacts with syndecan-2 and regulates neuronal morphology." *J Cell Biol* 193 (4):769-84. doi: 10.1083/jcb.201008050.

Chia, P. H., B. Chen, P. Li, M. K. Rosen, and K. Shen. 2014. "Local F-actin network links synapse formation and axon branching." *Cell* 156 (1-2):208-20. doi: 10.1016/j.cell.2013.12.009.

Coen, K., D. Pareyson, M. Auer-Grumbach, G. Buyse, N. Goemans, K. G. Claeys, N. Verpoorten, M. Laurà, V. Scaioli, W. Salmhofer, T. R. Pieber, E. Nelis, P. De Jonghe, and V. Timmerman. 2006. "Novel mutations in the HSN2 gene causing hereditary sensory and autonomic neuropathy type II." *Neurology* 66 (5):748-51. doi: 10.1212/01.wnl.0000201191.57519.47.

Coleman, M. P., and M. R. Freeman. 2010. "Wallerian degeneration, wld(s), and nmnat." *Annu Rev Neurosci* 33:245-67. doi: 10.1146/annurev-neuro-060909-153248.

Conforti, L., J. Gilley, and M. P. Coleman. 2014. "Wallerian degeneration: an emerging axon death pathway linking injury and disease." *Nat Rev Neurosci* 15 (6):394-409. doi: 10.1038/nrn3680.

Costa, A. M., F. Pinto, O. Martinho, M. J. Oliveira, P. Jordan, and R. M. Reis. 2015. "Silencing of the tumor suppressor gene WNK2 is associated with upregulation of MMP2 and JNK in gliomas." *Oncotarget* 6 (3):1422-34. doi: 10.18632/oncotarget.2805.

Courchet, J., T. L. Lewis, S. Lee, V. Courchet, D. Y. Liou, S. Aizawa, and F. Polleux. 2013. "Terminal axon branching is regulated by the LKB1-NUAK1 kinase pathway via

presynaptic mitochondrial capture." *Cell* 153 (7):1510-25. doi: 10.1016/j.cell.2013.05.021.
Dascenco, D., M. L. Erfurth, A. Izadifar, M. Song, S. Sachse, R. Bortnick, O. Urwyler, M. Petrovic, D. Ayaz, H. He, Y. Kise, F. Thomas, T. Kidd, and D. Schmucker. 2015. "Slit and Receptor Tyrosine Phosphatase 69D Confer Spatial Specificity to Axon Branching via Dscam1." *Cell* 162 (5):1140-54. doi: 10.1016/j.cell.2015.08.003.
Essuman, K., D. W. Summers, Y. Sasaki, X. Mao, A. DiAntonio, and J. Milbrandt. 2017. "The SARM1 Toll/Interleukin-1 Receptor Domain Possesses Intrinsic NAD." *Neuron* 93 (6):1334-1343.e5. doi: 10.1016/j.neuron.2017.02.022.
Fang, Y., L. Soares, X. Teng, M. Geary, and N. M. Bonini. 2012. "A novel Drosophila model of nerve injury reveals an essential role of Nmnat in maintaining axonal integrity." *Curr Biol* 22 (7):590-5. doi: 10.1016/j.cub.2012.01.065.
Gagnon, K. B., R. England, and E. Delpire. 2006. "Volume sensitivity of cation-Cl- cotransporters is modulated by the interaction of two kinases: Ste20-related proline-alanine-rich kinase and WNK4." *Am J Physiol Cell Physiol* 290 (1):C134-42. doi: 10.1152/ajpcell.00037.2005.
Gallolu Kankanamalage, S., A. S. Karra, and M. H. Cobb. 2018. "WNK pathways in cancer signaling networks." *Cell Commun Signal* 16 (1):72. doi: 10.1186/s12964-018-0287-1.
Garrity, P. A., C. H. Lee, I. Salecker, H. C. Robertson, C. J. Desai, K. Zinn, and S. L. Zipursky. 1999. "Retinal axon target selection in Drosophila is regulated by a receptor protein
Gerdts, J., E. J. Brace, Y. Sasaki, A. DiAntonio, and J. Milbrandt. 2015. "SARM1 activation triggers axon degeneration locally via NAD^+ destruction." *Science* 348 (6233):453-7. doi: 10.1126/science.1258366.
Gilley, J., R. Adalbert, G. Yu, and M. P. Coleman. 2013. "Rescue of peripheral and CNS axon defects in mice lacking NMNAT2." *J Neurosci* 33 (33):13410-24. doi: 10.1523/JNEUROSCI.1534-13.2013.
Gilley, J., and M. P. Coleman. 2010. "Endogenous Nmnat2 is an essential survival factor for maintenance of healthy axons." *PLoS Biol* 8 (1):e1000300. doi: 10.1371/journal.pbio.1000300.
Hadchouel, J., D. H. Ellison, and G. Gamba. 2016. "Regulation of Renal Electrolyte Transport by WNK and SPAK-OSR1 Kinases." *Annu Rev Physiol* 78:367-89. doi: 10.1146/annurev-physiol-021115-105431.
Hand, R., and F. Polleux. 2011. "Neurogenin2 regulates the initial axon guidance of cortical pyramidal neurons projecting medially to the corpus callosum." *Neural Dev* 6:30. doi: 10.1186/1749-8104-6-30.
He, H., Y. Kise, A. Izadifar, O. Urwyler, D. Ayaz, A. Parthasarthy, B. Yan, M. L. Erfurth, D. Dascenco, and D. Schmucker. 2014. "Cell-intrinsic requirement of Dscam1 isoform diversity for axon collateral formation." *Science* 344 (6188):1182-6. doi: 10.1126/science.1251852.
Hinz, U., B. Giebel, and J. A. Campos-Ortega. 1994. "The basic-helix-loop-helix domain of Drosophila lethal of scute protein is sufficient for proneural function and activates neurogenic genes." *Cell* 76 (1):77-87. doi: 10.1016/0092-8674(94)90174-0.
Hong, C., K. S. Moorefield, P. Jun, K. D. Aldape, S. Kharbanda, H. S. Phillips, and J. F. Costello. 2007. "Epigenome scans and cancer genome sequencing converge on WNK2, a kinase-independent suppressor of cell growth." *Proc Natl Acad Sci U S A* 104 (26):10974-9. doi: 10.1073/pnas.0700683104.
Hoopfer, E. D., T. McLaughlin, R. J. Watts, O. Schuldiner, D. D. O'Leary, and L. Luo. 2006. "Wlds protection distinguishes axon degeneration following injury from naturally occurring developmental pruning." *Neuron* 50 (6):883-95. doi: 10.1016/j.neuron.2006.05.013.
Hoorn, E. J., J. H. Nelson, J. A. McCormick, and D. H. Ellison. 2011. "The WNK kinase network regulating sodium, potassium, and blood pressure." *J Am Soc Nephrol* 22 (4):605-14. doi: 10.1681/ASN.2010080827.
Huppke, P., E. Wegener, J. Gilley, C. Angeletti, I. Kurth, J. P. H. Drenth, C. Stadelmann, A. Barrantes-Freer, W. Brück, H. Thiele, P. Nürnberg, J. Gärtner, G. Orsomando, and M. P. Coleman. 2019. "Homozygous NMNAT2 mutation in sisters with polyneuropathy and erythromelalgia." *Exp Neurol* 320:112958. doi: 10.1016/j.expneurol.2019.112958.

Iascone, D. M., Y. Li, U. Sümbül, M. Doron, H. Chen, V. Andreu, F. Goudy, H. Blockus, L. F. Abbott, I. Segev, H. Peng, and F. Polleux. 2020. "Whole-Neuron Synaptic Mapping Reveals Spatially Precise Excitatory/Inhibitory Balance Limiting Dendritic and Somatic Spiking." *Neuron* 106 (4):566-578.e8. doi: 10.1016/j.neuron.2020.02.015.

Jun, P., C. Hong, A. Lal, J. M. Wong, M. W. McDermott, A. W. Bollen, C. Plass, W. A. Held, D. J. Smiraglia, and J. F. Costello. 2009. "Epigenetic silencing of the kinase tumor suppressor WNK2 is tumor-type and tumor-grade specific." *Neuro Oncol* 11 (4):414-22. doi: 10.1215/15228517-2008-096.

Lafreniere, R. G., M. L. MacDonald, M. P. Dube, J. MacFarlane, M. O'Driscoll, B. Brais, S. Meilleur, R. R. Brinkman, O. Dadivas, T. Pape, C. Platon, C. Radomski, J. Risler, J. Thompson, A. M. Guerra-Escobio, G. Davar, X. O. Breakefield, S. N. Pimstone, R. Green, W. Pryse-Phillips, Y. P. Goldberg, H. B. Younghusband, M. R. Hayden, R. Sherrington, G. A. Rouleau, and M. E. Samuels. 2004. "Identification of a novel gene (HSN2) causing hereditary sensory and autonomic neuropathy type II through the Study of Canadian Genetic Isolates." *Am J Hum Genet* 74 (5):1064-73. doi: 10.1086/420795.

Lewis, T. L., G. F. Turi, S. K. Kwon, A. Losonczy, and F. Polleux. 2016. "Progressive Decrease of Mitochondrial Motility during Maturation of Cortical Axons In Vitro and In Vivo." *Curr Biol* 26 (19):2602-2608. doi: 10.1016/j.cub.2016.07.064.

Lewis, T. L., J. Courchet, and F. Polleux. 2013. "Cell biology in neuroscience: Cellular and molecular mechanisms underlying axon formation, growth, and branching." *J Cell Biol* 202 (6):837-48. doi: 10.1083/jcb.201305098.

Lukacs, M., J. Gilley, Y. Zhu, G. Orsomando, C. Angeletti, J. Liu, X. Yang, J. Park, R. J. Hopkin, M. P. Coleman, R. G. Zhai, and R. W. Stottmann. 2019. "Severe biallelic loss-of-function mutations in nicotinamide mononucleotide adenylyltransferase 2 (NMNAT2) in two fetuses with fetal akinesia deformation sequence." *Exp Neurol* 320:112961. doi: 10.1016/j.expneurol.2019.112961.

Matsuda, T., and C. L. Cepko. 2007. "Controlled expression of transgenes introduced by in vivo electroporation." *Proc Natl Acad Sci U S A* 104 (3):1027-32. doi: 10.1073/pnas.0610155104.

McCormick, J. A., and D. H. Ellison. 2011. "The WNKs: atypical protein kinases with pleiotropic actions." *Physiol Rev* 91 (1):177-219. doi: 10.1152/physrev.00017.2010.

Meyer-Dilhet, G., and J. Courchet. 2020. "In Utero Cortical Electroporation of Plasmids in the Mouse Embryo." *STAR Protoc* 1 (1):100027. doi: 10.1016/j.xpro.2020.100027.

Milde, S., J. Gilley, and M. P. Coleman. 2013. "Subcellular localization determines the stability and axon protective capacity of axon survival factor Nmnat2." *PLoS Biol* 11 (4):e1001539. doi: 10.1371/journal.pbio.1001539.

Moriguchi, T., S. Urushiyama, N. Hisamoto, S. Iemura, S. Uchida, T. Natsume, K. Matsumoto, and H. Shibuya. 2005. "WNK1 regulates phosphorylation of cation-chloride-coupled cotransporters via the STE20-related kinases, SPAK and OSR1." *J Biol Chem* 280 (52):42685-93. doi: 10.1074/jbc.M510042200.

Munemasa, Y., and Y. Kitaoka. 2015. "Autophagy in axonal degeneration in glaucomatous optic neuropathy." *Prog Retin Eye Res* 47:1-18. doi: 10.1016/j.preteyeres.2015.03.002.

Neukomm, L. J., T. C. Burdett, A. M. Seeds, S. Hampel, J. C. Coutinho-Budd, J. E. Farley, J. Wong, Y. B. Karadeniz, J. M. Osterloh, A. E. Sheehan, and M. R. Freeman. 2017. "Axon Death Pathways Converge on Axundead to Promote Functional and Structural Axon Disassembly." *Neuron* 95 (1):78-91.e5. doi: 10.1016/j.neuron.2017.06.031.

Osterloh, J. M., J. Yang, T. M. Rooney, A. N. Fox, R. Adalbert, E. H. Powell, A. E. Sheehan, M. A. Avery, R. Hackett, M. A. Logan, J. M. MacDonald, J. S. Ziegenfuss, S. Milde, Y. J. Hou, C. Nathan, A. Ding, R. H. Brown, L. Conforti, M. Coleman, M. Tessier-Lavigne, S. Züchner, and M. R. Freeman. 2012. "dSarm/Sarm1 is required for activation of an injury-induced axon death pathway." *Science* 337 (6093):481-4. doi: 10.1126/science.1223899.

Pela, I. 2012. "Familial Hyperkalemic Hypertension: A New Early-onset Pediatric Case." *Clin Pediatr Endocrinol* 21 (1):5-9. doi: 10.1297/cpe.21.5.

Pfeiffer, B. D., A. Jenett, A. S. Hammonds, T. T. Ngo, S. Misra, C. Murphy, A. Scully, J. W. Carlson, K. H. Wan, T. R. Laverty, C. Mungall, R. Svirskas, J. T. Kadonaga, C. Q. Doe, M. B. Eisen, S. E. Celniker, and G. M. Rubin. 2008. "Tools for neuroanatomy and

neurogenetics in Drosophila." *Proc Natl Acad Sci U S A* 105 (28):9715-20. doi: 10.1073/pnas.0803697105.

Polleux, F., and A. Ghosh. 2002. "The slice overlay assay: a versatile tool to study the influence of extracellular signals on neuronal development." *Sci STKE* 2002 (136):pl9. doi: 10.1126/stke.2002.136.pl9.

Raff, M. C., A. V. Whitmore, and J. T. Finn. 2002. "Axonal self-destruction and neurodegeneration." *Science* 296 (5569):868-71. doi: 10.1126/science.1068613.

Rafiqi, F. H., A. M. Zuber, M. Glover, C. Richardson, S. Fleming, S. Jovanović, A. Jovanović, K. M. O'Shaughnessy, and D. R. Alessi. 2010. "Role of the WNK-activated SPAK kinase in regulating blood pressure." *EMBO Mol Med* 2 (2):63-75. doi: 10.1002/emmm.200900058.

Rahmani, B., F. Fekrmandi, K. Ahadi, T. Ahadi, A. Alavi, A. Ahmadiani, and S. Asadi. 2018. "A novel nonsense mutation in WNK1/HSN2 associated with sensory neuropathy and limb destruction in four siblings of a large Iranian pedigree." *BMC Neurol* 18 (1):195. doi: 10.1186/s12883-018-1201-6.

Richardson, C., and D. R. Alessi. 2008. "The regulation of salt transport and blood pressure by the WNK-SPAK/OSR1 signalling pathway." *J Cell Sci* 121 (Pt 20):3293-304. doi: 10.1242/jcs.029223.

Richardson, C., F. H. Rafiqi, H. K. Karlsson, N. Moleleki, A. Vandewalle, D. G. Campbell, N. A. Morrice, and D. R. Alessi. 2008. "Activation of the thiazide-sensitive Na+-Cl- cotransporter by the WNK-regulated kinases SPAK and OSR1." *J Cell Sci* 121 (Pt 5):675-84. doi: 10.1242/jcs.025312.

Rivière, J. B., D. J. Verlaan, M. Shekarabi, R. G. Lafrenière, M. Bénard, V. M. Der Kaloustian, Z. Shbaklo, and G. A. Rouleau. 2004. "A mutation in the HSN2 gene causes sensory neuropathy type II in a Lebanese family." *Ann Neurol* 56 (4):572-5. doi: 10.1002/ana.20237.

Roddier, K., T. Thomas, G. Marleau, A. M. Gagnon, M. J. Dicaire, A. St-Denis, I. Gosselin, A. M. Sarrazin, A. Larbrisseau, M. Lambert, M. Vanasse, D. Gaudet, G. A. Rouleau, and B. Brais. 2005. "Two mutations in the HSN2 gene explain the high prevalence of HSAN2 in French Canadians." *Neurology* 64 (10):1762-7. doi: 10.1212/01.WNL.0000161849.29944.43.

Rual, J. F., J. Ceron, J. Koreth, T. Hao, A. S. Nicot, T. Hirozane-Kishikawa, J. Vandenhaute, S. H. Orkin, D. E. Hill, S. van den Heuvel, and M. Vidal. 2004. "Toward improving Caenorhabditis elegans phenome mapping with an ORFeome-based RNAi library." *Genome Res* 14 (10B):2162-8. doi: 10.1101/gr.2505604.

Ruan, K., Y. Zhu, C. Li, J. M. Brazill, and R. G. Zhai. 2015. "Alternative splicing of Drosophila Nmnat functions as a switch to enhance neuroprotection under stress." *Nat Commun* 6:10057. doi: 10.1038/ncomms10057.

Sachse, S. M., S. Lievens, L. F. Ribeiro, D. Dascenco, D. Masschaele, K. Horré, A. Misbaer, N. Vanderroost, A. S. De Smet, E. Salta, M. L. Erfurth, Y. Kise, S. Nebel, W. Van Delm, S. Plaisance, J. Tavernier, B. De Strooper, J. De Wit, and D. Schmucker. 2019. "Nuclear import of the DSCAM-cytoplasmic domain drives signaling capable of inhibiting synapse formation." *EMBO J* 38 (6). doi: 10.15252/embj.201899669.

Sasaki, Y., T. Nakagawa, X. Mao, A. DiAntonio, and J. Milbrandt. 2016. "NMNAT1 inhibits axon degeneration via blockade of SARM1-mediated NAD." *Elife* 5. doi: 10.7554/eLife.19749.

Sato, A., and H. Shibuya. 2018. "Glycogen synthase kinase 3ß functions as a positive effector in the WNK signaling pathway." *PLoS One* 13 (3):e0193204. doi: 10.1371/journal.pone.0193204.

Schneider, C. A., W. S. Rasband, and K. W. Eliceiri. 2012. "NIH Image to ImageJ: 25 years of image analysis." Nat Methods 9 (7):671-5. doi: 10.1038/nmeth.2089.

Shekarabi, M., N. Girard, J. B. Rivière, P. Dion, M. Houle, A. Toulouse, R. G. Lafrenière, F. Vercauteren, P. Hince, J. Laganiere, D. Rochefort, L. Faivre, M. Samuels, and G. A. Rouleau. 2008. "Mutations in the nervous system--specific HSN2 exon of WNK1 cause hereditary sensory neuropathy type II." *J Clin Invest* 118 (7):2496-505. doi: 10.1172/JCI34088.

Shekarabi, M., J. Zhang, A. R. Khanna, D. H. Ellison, E. Delpire, and K. T. Kahle. 2017. "WNK Kinase Signaling in Ion Homeostasis and Human Disease." *Cell Metab* 25 (2):285-299. doi: 10.1016/j.cmet.2017.01.007.

Siew, K., and K. M. O'Shaughnessy. 2013. "Extrarenal roles of the with-no-lysine[K] kinases (WNKs)." *Clin Exp Pharmacol Physiol* 40 (12):885-94. doi: 10.1111/1440-1681.12108.

Srahna, M., M. Leyssen, C. M. Choi, L. G. Fradkin, J. N. Noordermeer, and B. A. Hassan. 2006. "A signaling network for patterning of neuronal connectivity in the Drosophila brain." PLoS Biol 4 (11):e348. doi: 10.1371/journal.pbio.0040348.

Sudarsanam, S., S. Yaniv, H. Meltzer, and O. Schuldiner. 2020. "Cofilin regulates axon growth and branching of." *J Cell Sci* 133 (8). doi: 10.1242/jcs.232595.

Südhof, T. C. 2017. "Molecular Neuroscience in the 21." *Neuron* 96 (3):536-541. doi: 10.1016/j.neuron.2017.10.005.

Urwyler, O., A. Izadifar, D. Dascenco, M. Petrovic, H. He, D. Ayaz, A. Kremer, S. Lippens, P. Baatsen, C. J. Guérin, and D. Schmucker. 2015. "Investigating CNS synaptogenesis at single-synapse resolution by combining reverse genetics with correlative light and electron microscopy." *Development* 142 (2):394-405. doi: 10.1242/dev.115071.

Urwyler, O., A. Izadifar, S. Vandenbogaerde, S. Sachse, A. Misbaer, and D. Schmucker. 2019. "Branch-restricted localization of phosphatase Prl-1 specifies axonal synaptogenesis domains." *Science* 364 (6439). doi: 10.1126/science.aau9952.

Veríssimo, F., and P. Jordan. 2001. "WNK kinases, a novel protein kinase subfamily in multi-cellular organisms." *Oncogene* 20 (39):5562-9. doi: 10.1038/sj.onc.1204726.

Vidal-Petiot, E., E. Elvira-Matelot, K. Mutig, C. Soukaseum, V. Baudrie, S. Wu, L. Cheval, E. Huc, M. Cambillau, S. Bachmann, A. Doucet, X. Jeunemaitre, and J. Hadchouel. 2013. "WNK1-related Familial Hyperkalemic Hypertension results from an increased expression of L-WNK1 specifically in the distal nephron." *Proc Natl Acad Sci U S A* 110 (35):14366-71. doi: 10.1073/pnas.1304230110.

Vitari, A. C., M. Deak, N. A. Morrice, and D. R. Alessi. 2005. "The WNK1 and WNK4 protein kinases that are mutated in Gordon's hypertension syndrome phosphorylate and activate SPAK and OSR1 protein kinases." *Biochem J* 391 (Pt 1):17-24. doi: 10.1042/BJ20051180.

Vohra, B. P., Y. Sasaki, B. R. Miller, J. Chang, A. DiAntonio, and J. Milbrandt. 2010. "Amyloid precursor protein cleavage-dependent and -independent axonal degeneration programs share a common nicotinamide mononucleotide adenylyltransferase 1-sensitive pathway." *J Neurosci* 30 (41):13729-38. doi: 10.1523/JNEUROSCI.2939-10.2010.

Wen, Y., J. Z. Parrish, R. He, R. G. Zhai, and M. D. Kim. 2011. "Nmnat exerts neuroprotective effects in dendrites and axons." *Mol Cell Neurosci* 48 (1):1-8. doi: 10.1016/j.mcn.2011.05.002.

Wilson, F. H., S. Disse-Nicodème, K. A. Choate, K. Ishikawa, C. Nelson-Williams, I. Desitter, M. Gunel, D. V. Milford, G. W. Lipkin, J. M. Achard, M. P. Feely, B. Dussol, Y. Berland, R. J. Unwin, H. Mayan, D. B. Simon, Z. Farfel, X. Jeunemaitre, and R. P. Lifton. 2001. "Human hypertension caused by mutations in WNK kinases." *Science* 293 (5532):1107-12. doi: 10.1126/science.1062844.

Wu, A., M. Wolley, and M. Stowasser. 2019. "The interplay of renal potassium and sodium handling in blood pressure regulation: critical role of the WNK-SPAK-NCC pathway." *J Hum Hypertens* 33 (7):508-523. doi: 10.1038/s41371-019-0170-6.

Xiong, X., Y. Hao, K. Sun, J. Li, X. Li, B. Mishra, P. Soppina, C. Wu, R. I. Hume, and C. A. Collins. 2012. "The Highwire ubiquitin ligase promotes axonal degeneration by tuning levels of Nmnat protein." *PLoS Biol* 10 (12):e1001440. doi: 10.1371/journal.pbio.1001440.

Xu, B., J. M. English, J. L. Wilsbacher, S. Stippec, E. J. Goldsmith, and M. H. Cobb. 2000. "WNK1, a novel mammalian serine/threonine protein kinase lacking the catalytic lysine in subdomain II." *J Biol Chem* 275 (22):16795-801. doi: 10.1074/jbc.275.22.16795.

Yang, C. L., J. Angell, R. Mitchell, and D. H. Ellison. 2003. "WNK kinases regulate thiazide-sensitive Na-Cl cotransport." *J Clin Invest* 111 (7):1039-45. doi: 10.1172/JCI17443.

Yang, J., Z. Wu, N. Renier, D. J. Simon, K. Uryu, D. S. Park, P. A. Greer, C. Tournier, R. J. Davis, and M. Tessier-Lavigne. 2015. "Pathological axonal death through a MAPK

cascade that triggers a local energy deficit." *Cell* 160 (1-2):161-76. doi: 10.1016/j.cell.2014.11.053.
Yuan, J. H., A. Hashiguchi, A. Yoshimura, N. Sakai, M. P. Takahashi, T. Ueda, A. Taniguchi, S. Okamoto, N. Kanazawa, Y. Yamamoto, K. Saigoh, S. Kusunoki, M. Ando, Y. Hiramatsu, Y. Okamoto, and H. Takashima. 2017. "WNK1/HSN2 founder mutation in patients with hereditary sensory and autonomic neuropathy: A Japanese cohort study." *Clin Genet* 92 (6):659-663. doi: 10.1111/cge.13037.
Zhai, R. G., F. Zhang, P. R. Hiesinger, Y. Cao, C. M. Haueter, and H. J. Bellen. 2008. "NAD synthase NMNAT acts as a chaperone to protect against neurodegeneration." *Nature* 452 (7189):887-91. doi: 10.1038/nature06721.

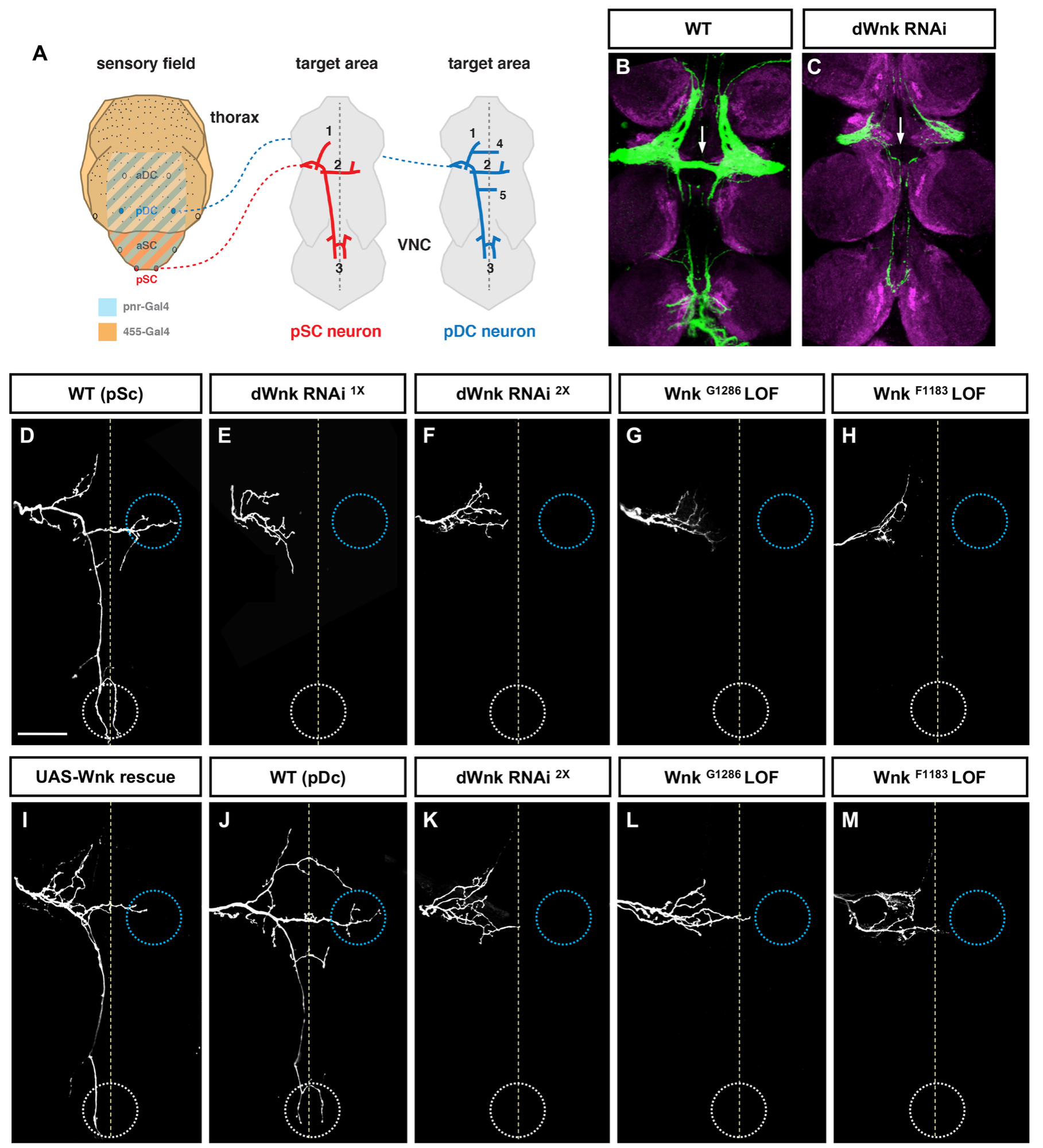
A
sensory field
target area
target area
thorax
aDC
pDC
aSC
pSC
1
2
3
1
4
2
5
3
VNC
pnr-Gal4
455-Gal4
pSC neuron
pDC neuron
WT
dWnk RNAi
B
C
WT (pSc)
dWnk RNAi 1X
dWnk RNAi 2X
Wnk G1286 LOF
Wnk F1183 LOF
D
E
F
G
H
UAS-Wnk rescue
WT (pDc)
dWnk RNAi 2X
Wnk G1286 LOF
Wnk F1183 LOF
I
J
K
L
M

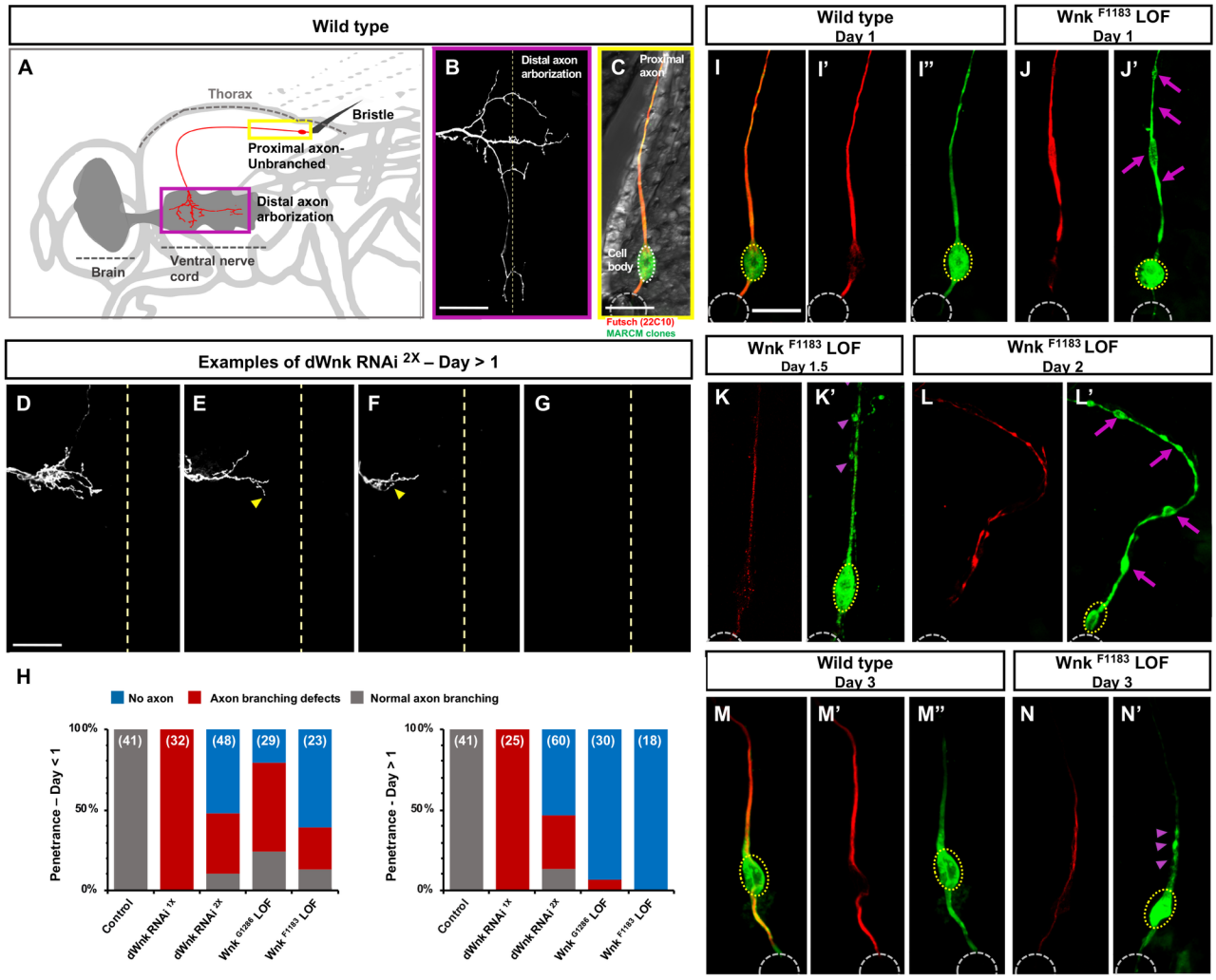
Wild type
A
Thorax
Bristle
Proximal axon-
Unbranched
Distal axon
arborization
Brain
Ventral nerve
cord
B
Distal axon
arborization
C
Proximal
axon
Cell
body
Futsch (22C10)
MARCM clones
Wild type
Day 1
Wnk F1183 LOF
Day 1
I
I'
I''
J
J'
Examples of dWnk RNAi 2X – Day > 1
D
E
F
G
Wnk F1183 LOF
Day 1.5
Wnk F1183 LOF
Day 2
K
K'
L
L'
H
No axon
Axon branching defects
Normal axon branching
Penetrance – Day < 1
100%
50%
0%
(41)
(32)
(48)
(29)
(23)
Control
dWnk RNAi 1X
dWnk RNAi 2X
Wnk G1286 LOF
Wnk F1183 LOF
Penetrance - Day > 1
100%
50%
0%
(41)
(25)
(60)
(30)
(18)
Control
dWnk RNAi 1X
dWnk RNAi 2X
Wnk G1286 LOF
Wnk F1183 LOF
Wild type
Day 3
Wnk F1183 LOF
Day 3
M
M'
M''
N
N'

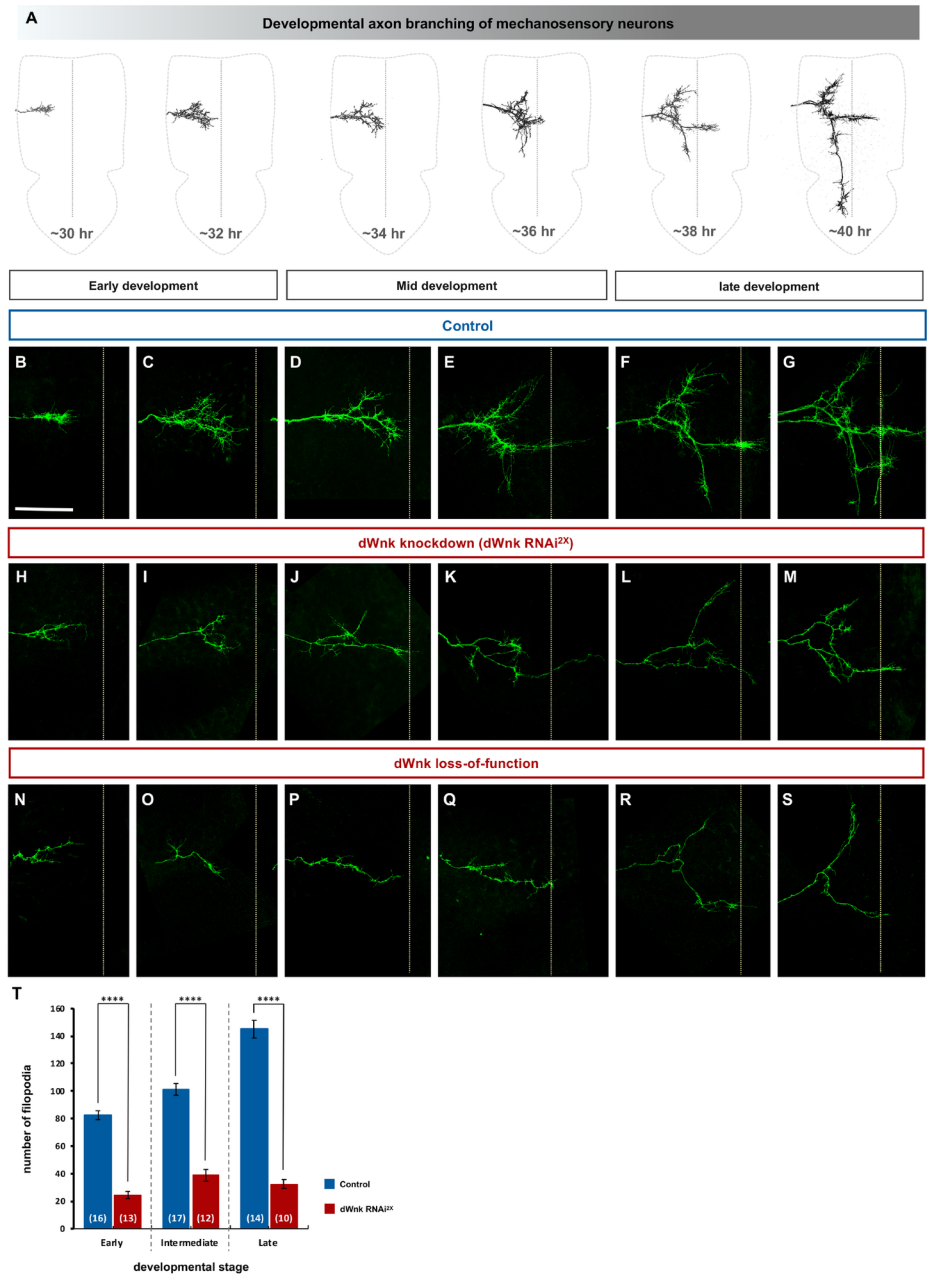
A
Developmental axon branching of mechanosensory neurons
~30 hr
~32 hr
~34 hr
~36 hr
~38 hr
~40 hr
Early development
Mid development
late development
Control
B
C
D
E
F
G
dWnk knockdown (dWnk RNAi2X)
H
I
J
K
L
M
dWnk loss-of-function
N
O
P
Q
R
S
T
number of filopodia
160
140
120
100
80
60
40
20
0
****
****
****
(16)
(13)
(17)
(12)
(14)
(10)
Early
Intermediate
Late
developmental stage
Control
dWnk RNAi2X

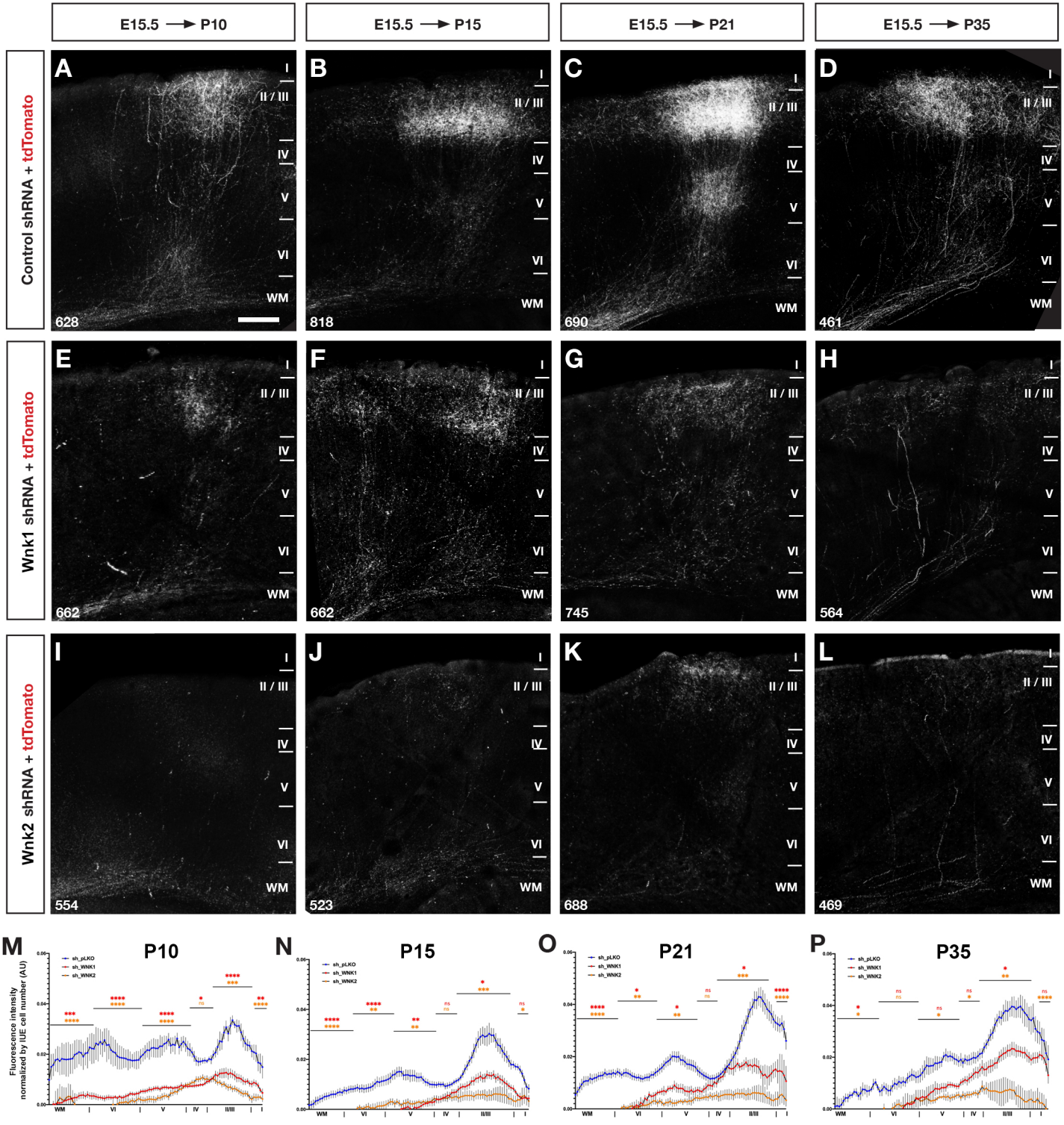
E15.5 → P10
E15.5 → P15
E15.5 → P21
E15.5 → P35
Control shRNA + tdTomato
Wnk1 shRNA + tdTomato
Wnk2 shRNA + tdTomato
A
B
C
D
E
F
G
H
I
J
K
L
I
II / III
IV
V
VI
WM
628
818
690
461
662
662
745
564
554
523
688
469
M
N
O
P
P10
P15
P21
P35
Fluorescence intensity normalized by IUE cell number (AU)
sh_pLKO
sh_WNK1
sh_WNK2
WM
VI
V
IV
II/III
I

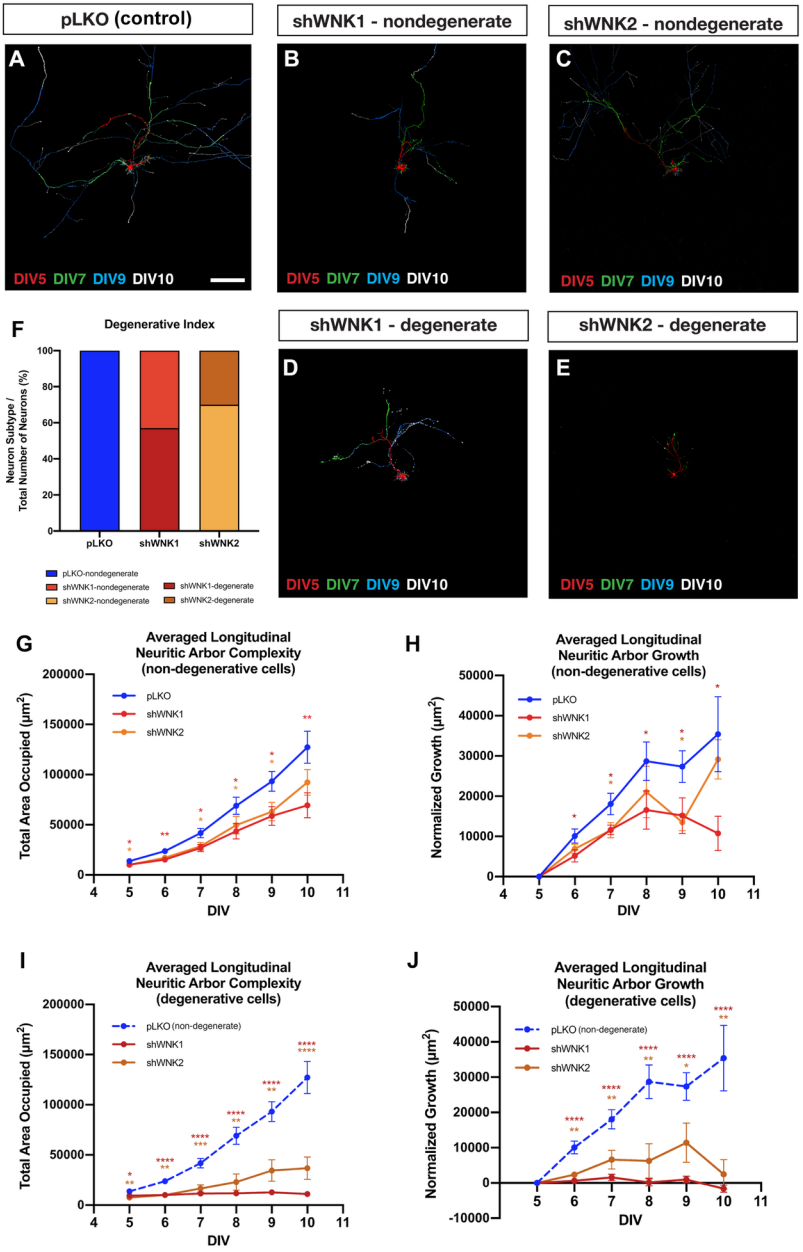
pLKO (control)
shWNK1 - nondegenerate
shWNK2 - nondegenerate
A
B
C
DIV5 DIV7 DIV9 DIV10
F
Degenerative Index
Neuron Subtype / Total Number of Neurons (%)
pLKO
shWNK1
shWNK2
pLKO-nondegenerate
shWNK1-nondegenerate
shWNK2-nondegenerate
shWNK1-degenerate
shWNK2-degenerate
shWNK1 - degenerate
shWNK2 - degenerate
D
E
G
Averaged Longitudinal Neuritic Arbor Complexity (non-degenerative cells)
Total Area Occupied (µm²)
DIV
H
Averaged Longitudinal Neuritic Arbor Growth (non-degenerative cells)
Normalized Growth (µm²)
I
Averaged Longitudinal Neuritic Arbor Complexity (degenerative cells)
pLKO (non-degenerate)
J
Averaged Longitudinal Neuritic Arbor Growth (degenerative cells)

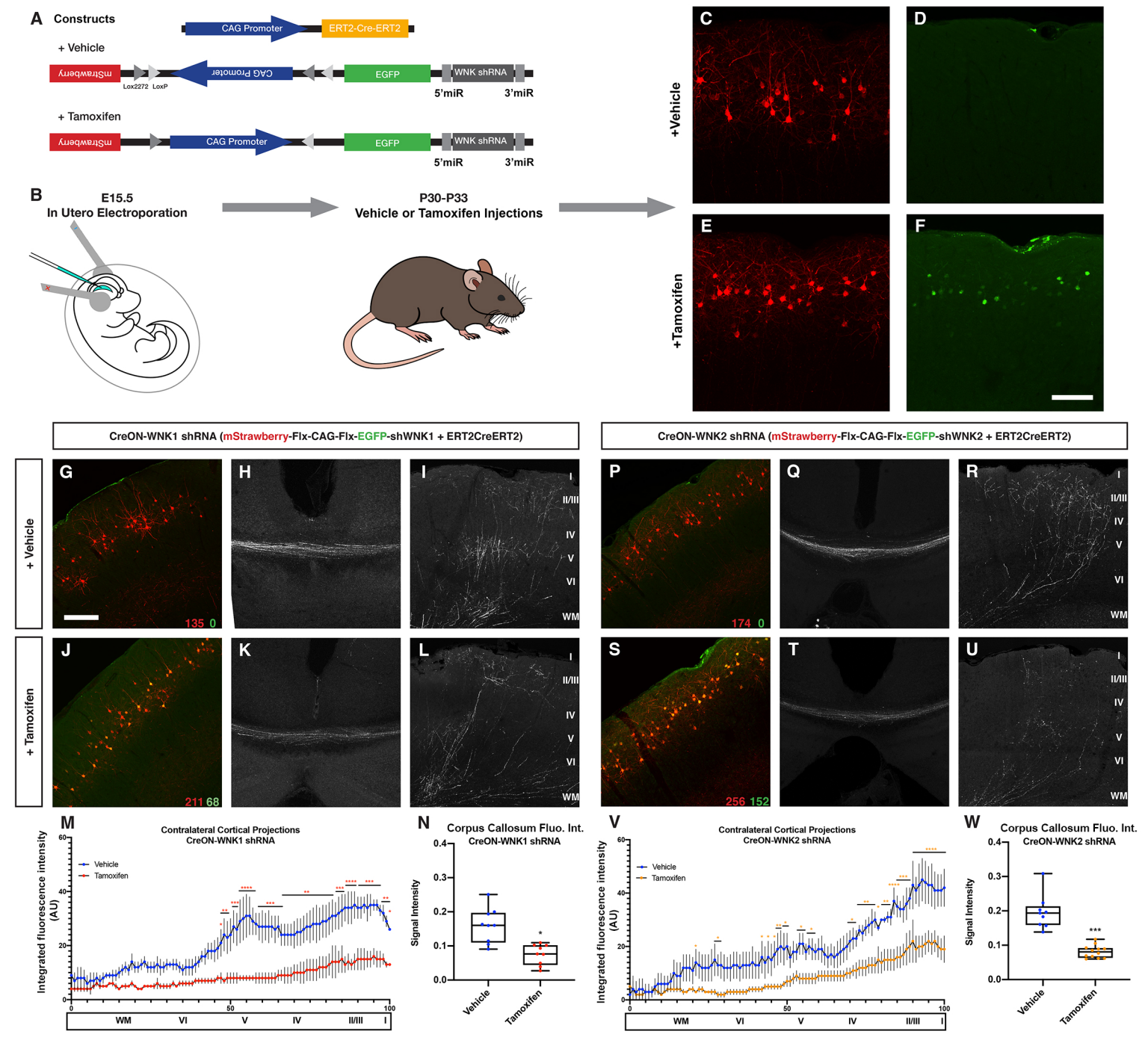
A
Constructs
CAG Promoter
ERT2-Cre-ERT2
+ Vehicle
mStrawberry
CAG Promoter
EGFP
WNK shRNA
Lox2272 LoxP
5'miR
3'miR
+ Tamoxifen
mStrawberry
CAG Promoter
EGFP
WNK shRNA
5'miR
3'miR
B
E15.5
In Utero Electroporation
P30-P33
Vehicle or Tamoxifen Injections
C
D
+Vehicle
E
F
+Tamoxifen
CreON-WNK1 shRNA (mStrawberry-Flx-CAG-Flx-EGFP-shWNK1 + ERT2CreERT2)
CreON-WNK2 shRNA (mStrawberry-Flx-CAG-Flx-EGFP-shWNK2 + ERT2CreERT2)
+ Vehicle
+ Tamoxifen
G
H
I
P
Q
R
J
K
L
S
T
U
135 0
211 68
174 0
256 152
I
II/III
IV
V
VI
WM
M
Contralateral Cortical Projections
CreON-WNK1 shRNA
Integrated fluorescence intensity (AU)
Vehicle
Tamoxifen
WM
VI
V
IV
II/III
I
N
Corpus Callosum Fluo. Int.
CreON-WNK1 shRNA
Signal Intensity
Vehicle
Tamoxifen
V
Contralateral Cortical Projections
CreON-WNK2 shRNA
Integrated fluorescence intensity (AU)
Vehicle
Tamoxifen
W
Corpus Callosum Fluo. Int.
CreON-WNK2 shRNA
Signal Intensity
Vehicle
Tamoxifen

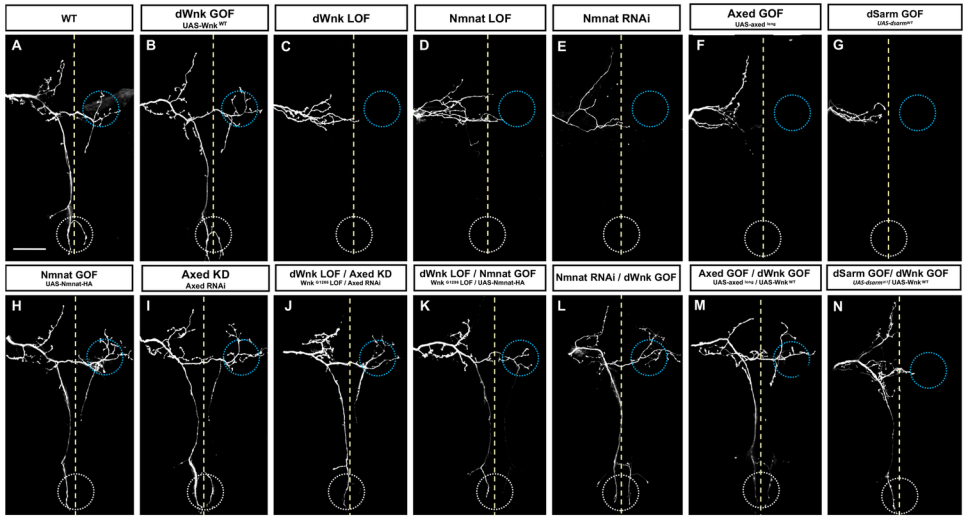
WT
dWnk GOF
UAS-Wnk WT
dWnk LOF
Nmnat LOF
Nmnat RNAi
Axed GOF
UAS-axed 1-ins
dSarm GOF
UAS-dsarm WT
A
B
C
D
E
F
G
Nmnat GOF
UAS-Nmnat-HA
Axed KD
Axed RNAi
dWnk LOF / Axed KD
Wnk 61199 LOF / Axed RNAi
dWnk LOF / Nmnat GOF
Wnk 61199 LOF / UAS-Nmnat-HA
Nmnat RNAi / dWnk GOF
Axed GOF / dWnk GOF
UAS-axed 1-ins / UAS-Wnk WT
dSarm GOF/ dWnk GOF
UAS-dsarm E1 UAS-Wnk WT
H
I
J
K
L
M
N

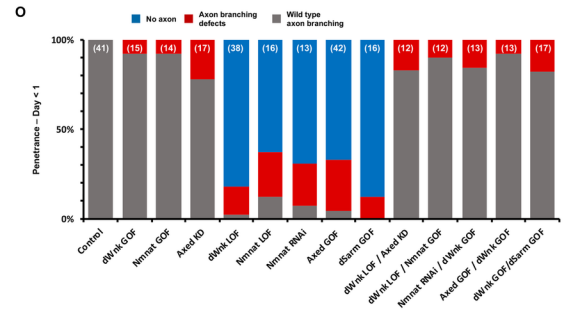
O
No axon
Axon branching defects
Wild type axon branching
Penetrance – Day < 1
100%
50%
0%
(41)
(15)
(14)
(17)
(38)
(16)
(13)
(42)
(16)
(12)
(12)
(13)
(13)
(17)
Control
dWnk GOF
Nmnat GOF
Axed KD
dWnk LOF
Nmnat LOF
Nmnat RNAi
Axed GOF
dSarm GOF
dWnk LOF / Axed KD
dWnk LOF / Nmnat GOF
Nmnat RNAi / dWnk GOF
Axed GOF / dWnk GOF
dWnk GOF /dSarm GOF

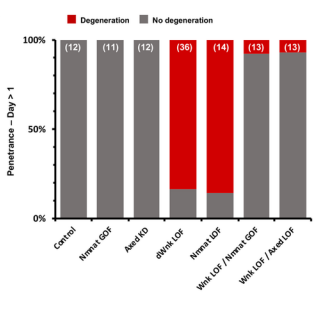
X
Degeneration
No degeneration
Penetrance – Day > 1
100%
50%
0%
(12)
(11)
(12)
(36)
(14)
(13)
(13)
Control
Nmnat GOF
Axed KD
dWnk LOF
Nmnat LOF
Wnk LOF / Nmnat GOF
Wnk LOF / Axed LOF

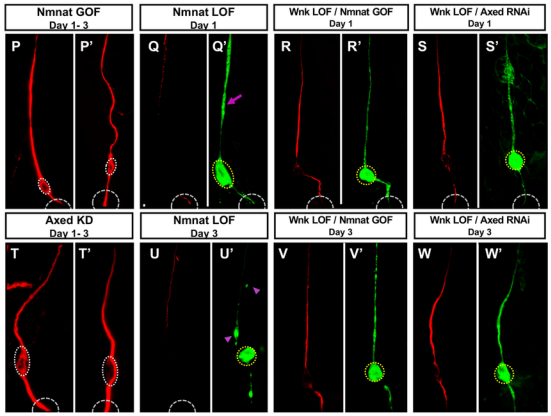
Nmnat GOF
Day 1- 3
Nmnat LOF
Day 1
Wnk LOF / Nmnat GOF
Day 1
Wnk LOF / Axed RNAi
Day 1
P
P'
Q
Q'
R
R'
S
S'
Axed KD
Day 1- 3
Nmnat LOF
Day 3
Wnk LOF / Nmnat GOF
Day 3
Wnk LOF / Axed RNAi
Day 3
T
T'
U
U'
V
V'
W
W'

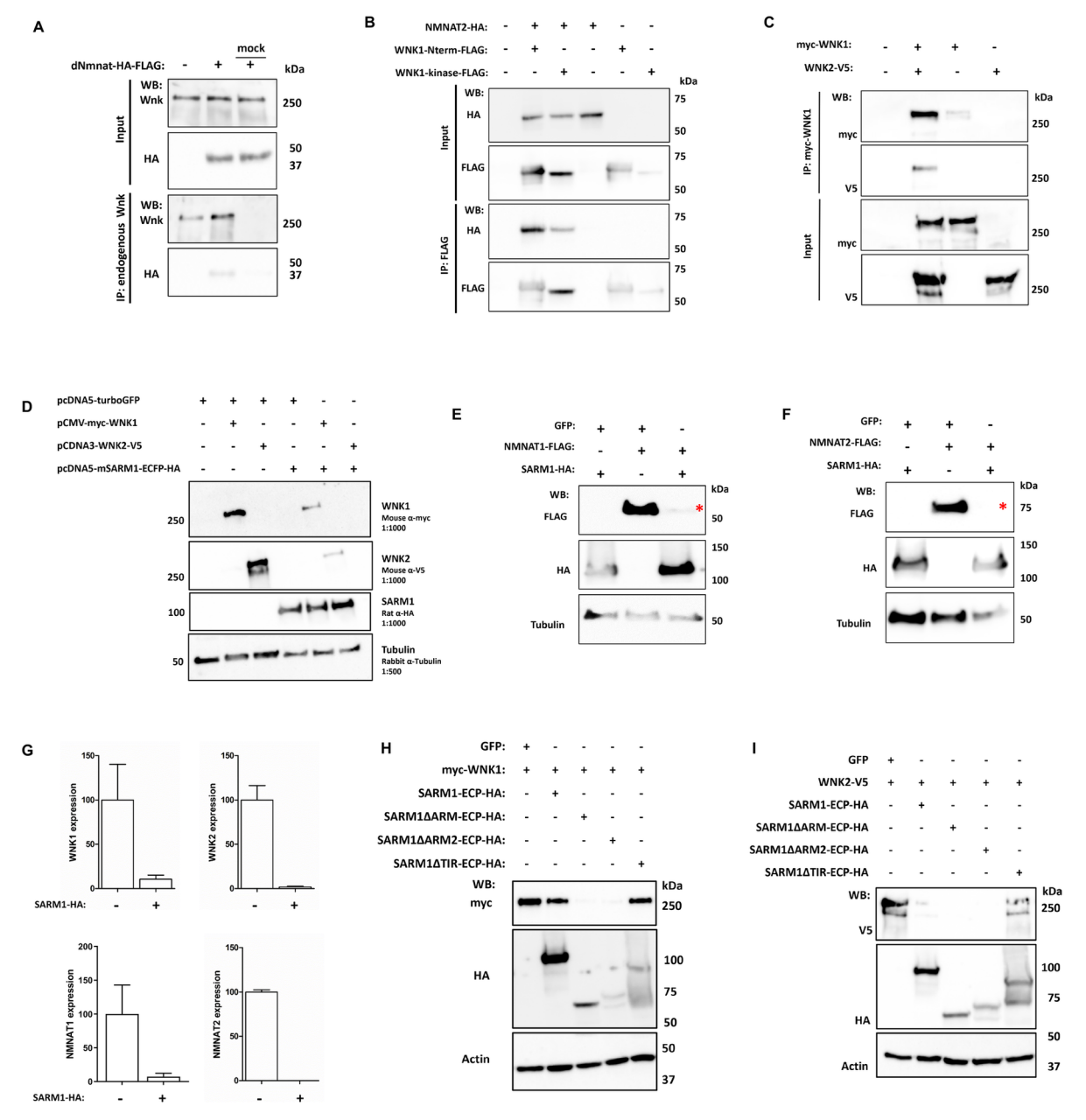
A
mock
dNmnat-HA-FLAG: - + +
kDa
Input
WB: Wnk
250
HA
50
37
IP: endogenous Wnk
WB: Wnk
250
HA
50
37
B
NMNAT2-HA: - + + + - -
WK1-Nterm-FLAG: - + - - + -
WK1-kinase-FLAG: - - + - - +
kDa
Input
WB: HA
75
50
FLAG
75
50
IP: FLAG
WB: HA
75
50
FLAG
75
50
C
myc-WNK1: - + + -
WNK2-V5: - + - +
IP: myc-WNK1
WB: myc
kDa
250
V5
250
Input
myc
250
V5
250
D
pcDNA5-turboGFP + + + + - -
pCMV-myc-WNK1 - + - - + -
pCDNA3-WNK2-V5 - - + - - +
pcDNA5-mSARM1-ECFP-HA - - - + + +
250
WNK1
Mouse α-myc
1:1000
250
WNK2
Mouse α-V5
1:1000
100
SARM1
Rat α-HA
1:1000
50
Tubulin
Rabbit α-Tubulin
1:500
E
GFP: + + -
NMNAT1-FLAG: - + +
SARM1-HA: + - +
WB:
kDa
FLAG
*
50
HA
150
100
Tubulin
50
F
GFP: + + -
NMNAT2-FLAG: - + +
SARM1-HA: + - +
WB:
kDa
FLAG
*
75
HA
150
100
Tubulin
50
G
WNK1 expression
150
100
50
0
WNK2 expression
150
100
50
0
SARM1-HA: - + - +
NMNAT1 expression
200
150
100
50
0
NMNAT2 expression
150
100
50
0
SARM1-HA: - + - +
H
GFP: + - - - -
myc-WNK1: + + + + +
SARM1-ECP-HA: - + - - -
SARM1ΔARM-ECP-HA: - - + - -
SARM1ΔARM2-ECP-HA: - - - + -
SARM1ΔTIR-ECP-HA: - - - - +
WB:
kDa
myc
250
HA
100
75
50
Actin
50
37
I
GFP + - - - -
WNK2-V5 + + + + +
SARM1-ECP-HA - + - - -
SARM1ΔARM-ECP-HA - - + - -
SARM1ΔARM2-ECP-HA - - - + -
SARM1ΔTIR-ECP-HA - - - - +
WB:
kDa
V5
250
HA
100
75
50
Actin
50
37